Title: Individualization of exosuit assistance based on measured muscle dynamics during versatile walking

Authors:

R. W. Nuckols[1*†], S. Lee[1†], K. Swaminathan[1†], D. Orzel[1], R. D. Howe[1], and C. J. Walsh[1*]

Affiliations:

[1]John A. Paulson School of Engineering and Applied Sciences and the Wyss Institute for Biologically Inspired Engineering, Harvard University; Cambridge, USA.

*Corresponding author. Email: rnuckols@seas.harvard.edu and walsh@seas.harvard.edu
†These authors contributed equally to this work.

Abstract: Variability in human walking depends upon individual physiology, environment, and walking task. Consequently, in the field of wearable robotics, there is a clear need for customizing assistance to the user and task. Here we developed a muscle-based assistance (MBA) strategy wherein exosuit assistance was derived from direct measurements of individuals' muscle dynamics during specific tasks. In this article, we recorded individuals' soleus muscle dynamics using ultrasonographic imaging during multiple walking speeds and inclines. From these pre-recorded images, we estimated the force produced by the soleus through inefficient concentric contraction and designed the exosuit assistance profile to be proportional to that estimated force. We evaluated this approach with a bilateral ankle exosuit at each measured walking task. Compared to not wearing a device, the MBA ankle exosuit significantly reduced metabolic demand by an average of 15.9%, 9.7%, 8.9% at level 1.25, 1.5, and 1.75 m s^{-1} respectively and 7.8% at 1.25 m s^{-1} at 5.71º incline while applying lower assistance levels than existing literature. In an additional study (*n*=2), we showed for multiple walking tasks that the MBA profile outperforms other bioinspired strategies and the average profile from a previous optimization study. Finally, we show the feasibility of online assistance generation in a mobile version for overground outdoor walking. This muscle-based approach enables relatively rapid (~10 seconds) generation of individualized low-force assistance profiles that provide metabolic benefit. This approach may help support the adoption of wearable robotics in real-world, dynamic locomotor tasks by enabling comfortable, tailored, and adaptive assistance.

One-Sentence Summary: An ankle exosuit tuned to the measured muscle dynamics of the user during multiple walking tasks improves energy economy.

Main Text:

INTRODUCTION

Wearable robotic systems have the potential for assisting locomotion in numerous areas including recreation, clinical rehabilitation and assistance, and occupations with demanding tasks. As the field moves towards designing for more widespread use and real-world applications, the effectiveness of systems will depend upon their ability to address variability in the human user and adapt to different tasks. Human walking is influenced by sex, height, body composition, age, and muscle strength (*1–6*), and can be further affected by neural or muscular disorders such as

stroke (*7*) or Parkinson's Disease (*8*). An individual's walking is also altered by the environment (*9–11*) and task (*12–14*).

50   The importance of human individuality and the need for customizing exoskeleton or exosuit assistance to the person and task is becoming increasingly clear in the field of wearable robotics. For the lower extremity, the leading approach for individualizing assistance profiles to the person is human-in-the-loop (HIL) optimization (*15*). By continuously measuring physiologic feedback of whole-body metabolic demand while individuals walk with assistance, the assistance profiles and parameters can be iteratively updated until metabolic demand is minimized. This approach has produced exciting results, significantly reducing the energy cost of walking (*15*, *16*) and running (*17*). However, while optimization is effective, it also requires a relatively long time (64-208 minutes) to converge on optimal parameters for even a single walking task (*e.g.* fixed speed and level ground) (*15*).

60   An alternative approach for assistance derives the profiles from biological mechanisms and aims to mimic the intent of the individual at a local joint or muscle level. By emulating the mechanics of the wearer, these biomechanistic strategies may enable increased versatility as the assistance is inherently reflective of the individual and how they adapt to locomotor tasks. Prior joint-level approaches have targeted joint moment, power, or key features of them (*e.g.* onset, peak, and offset timings of assistance) (*18–22*). Proportional surface electromyography (EMG)-based controllers measure the neural activation of a muscle and generate assistance profiles that are proportional to that neural activation profile (*23*, *24*). Studies using these bio-mechanistic approaches have shown that assisting specific muscles can lead to reductions in whole-body energetics, and at a local level, reduce biological joint moment, power, and muscle activity (*18–20*, *23*). Despite existing mechanistic approaches having benefits of individualization and adaptability, a limitation may be that they do not fully consider the underlying muscle-tendon (MT) dynamics (Fig. 1A), which cannot be entirely captured with conventional kinematic or EMG measurement techniques (*25*, *26*).

The ability of the ankle joint to efficiently produce the majority of positive power in walking (*26*) is linked to the ankle plantar flexor MTs. Over a gait cycle, the plantar flexor MTs with short pennate muscle fascicles and long compliant in-series tendons enables efficient storage and return of elastic mechanical energy (*27*). The neuromuscular system is tuned to permit this effective exchange of energy between the muscle, tendon, and environment. In level walking at 1.25 m s^{-1}, during early stance (~0-30% of the gait cycle), the plantar flexor muscle fascicles generate force
80   approximately isometrically, meaning that the muscle is not changing length and is acting like a mechanical clutch. By remaining approximately isometric, the muscle fascicle can operate under favorable force-velocity (F-V) contractile conditions where force production is economical (Fig. 1B). During this time region, the Achilles Tendon is also stretching and storing mechanical energy while the ankle dorsiflexes. Towards mid-stance (~40%), the muscle begins to contract concentrically (shorten) to add additional energy to the MT system. Finally, during late stance (~40-60%), the muscle continues to contract concentrically to generate additional positive power and the energy that was stored in the tendon is returned to generate positive power for push-off. The production of force during by concentric contraction is understood to be more metabolically costly than eccentric or isometric contraction due to reduced mechanochemical efficiency of ATP
90   synthesis (*28–30*).

These timings are average approximations for level walking at 1.25 m s^{-1}, but muscle-tendon dynamics vary across individuals and are task-dependent (*31*, *32*). As walking speed changes, fascicle shortening velocity changes to accommodate the demands (*26*, *33*). For uphill walking, positive power is needed to raise the center of mass; however, the relatively high compliance of the ankle MT makes it less effective in these tasks (*34*, *35*). By understanding how individuals take advantage of muscle-tendon mechanisms to produce efficient movement in a variety of activities, we have the opportunity to develop systems that work more synergistically with the user. We expect that an exosuit assistance strategy based on the individuals' measured muscle dynamics (*i.e.* force, power) in the specific task would improve exosuit performance and provide benefit during real-world use.

We developed a muscle-based assistance (MBA) strategy wherein the exosuit assistance was derived from direct measurements of soleus muscle dynamics from each participant as they walked in multiple walking tasks. We directly measured soleus muscle dynamics by using B-mode ultrasonography (US), which captured a continuous sequence of 2-D images of the soleus as participants walked. For each individual and task, we pre-recorded B-mode US images and estimated the force produced by the soleus during the inefficient concentric contraction phase. We then designed the exosuit assistance profile to be proportional to that estimated force. This approach allowed us to separate the force generation developed through efficient passive tendon mechanics and economical isometric muscle contraction, from the force that is generated uneconomically when the muscle concentrically contracts (*i.e.* shortening and producing positive power). We focus only on the soleus muscle as it is the largest of the plantar flexor muscles, making up approximately 54% of the physiological area (*36*). This was done to simplify the approach and to aim for the lowest level of force that provides appreciable benefit.

We developed and tested the MBA approach with a bilateral ankle soft exosuit at multiple walking speeds (1.0, 1.25, 1.5, and 1.75 m s^{-1}) and incline walking (1.25 m s^{-1} at a 5.71° incline). Our goal was to assess if the bilateral ankle assistance with the MBA profile would be effective in reducing the metabolic energy demand for these walking tasks compared to not wearing a device. To further reinforce our investigation into the effectiveness of the MBA profile, we performed an additional study that directly compared the MBA profile to other bioinspired strategies and the average profile from a previous optimization study with high assistance levels (*15*, *37*). We also performed a single-participant study where we used US to directly measure the effects of MBA assistance on muscle dynamics. Finally, we performed a proof-of-concept study demonstrating the feasibility of online MBA assistance generation in a mobile ankle exosuit for overground outdoor walking.

RESULTS

Muscle-Dynamics Based Assistance Profile Generation.

We measured B-mode ultrasound (US), joint kinematics and kinetics, and EMG on nine healthy adults (*n*=9, 3F 6M; age = 29.1 ± 4.04 yrs (mean ± std); mass = 67.9 ± 12.9 kg; height = 1.71 ± 0.07 m) while they walked at speeds of 1.0, 1.25, 1.5, and 1.75 m s^{-1} on level ground and additionally at 1.25 m s^{-1} at a 5.71° (10% grade) incline. From these data, we calculated the task-specific assistance profiles for each participant that were designed to mimic the demand for

concentric contraction in the muscle (Fig. 2, Fig. S1). As level ground walking speed increased, the exosuit profiles exhibited earlier force development and higher force magnitude. Similarly, compared to level walking, uphill walking profiles at matched speed developed force earlier and had higher force magnitude (Fig. 3A, Fig. S2, Table S1).

To highlight the importance of evaluating the underlying muscle in developing individual and task-specific profiles, we analyzed how the joint and the estimated muscle dynamics changed across conditions and participants. The response to changing tasks varied more in the muscle than at the joint. Compared to level 1.25 m s^{-1}, MBA force at 60% of the gait cycle changed by -39.4%, 61.3%, 121.2% and 99.9% for 1.0, 1.5, and 1.75 m s^{-1} and 5.71° incline (Fig. 3A, Fig. S2, Table S1). The ankle joint produced relatively similar moments across walking speeds and inclines and was similar across participants. Compared to level 1.25 m s^{-1}, peak ankle joint moment changed by -9.3%, 8.7%, 17.2% and 13.1% for 1.0, 1.5, and 1.75 m s^{-1} and 5.71° incline. Peak ankle power was more sensitive across walking speeds with a difference of -29.2%, 26.1%, 54.2% for 1.0, 1.5, and 1.75 m s^{-1} compared to 1.25 m s^{-1}, but was less sensitive to incline, which increased by 19.5% for 5.71° (Fig. 3A, Fig. S2, Table S2). Moreover, the onset of positive muscle power was more sensitive to the walking task than the onset of positive joint power (Table S1).

There was a slight negative but non-significant correlation between peak MBA exosuit torque (non-mass normalized) and body mass (Two-way ANOVA; Main effect: mass $p=0.2409$; task $p<0.0001$; $R^2 = 0.56$).

Effect of MBA Profile on Metabolic Demand in Multiple Walking Tasks.

We tested if the MBA method was effective at reducing metabolic energy demand. Following a training session, the nine participants walked in the same walking tasks with the ankle exosuit applying plantar flexion assistance using the individualized and task-specific MBA profiles (Fig. 3B). The peak applied torque was 0.18 ± 0.03, 0.23 ± 0.03, 0.30 ± 0.03, 0.33 ± 0.03, and 0.38 ± 0.03 N m kg^{-1} for 1.00, 1.25, 1.5, 1.75 m s^{-1} and 5.71° walking respectively (Table S2). The MBA approach allowed us to develop assistance profiles that were effective across a range of walking tasks. Compared to NO-DEVICE, the exosuit with the MBA profiles significantly reduced the metabolic demand for level walking at 1.25, 1.5, and 1.75 m s^{-1} and for 5.71° incline walking at 1.25 m s^{-1}. The net metabolic reduction comparing MBA to NO-DEVICE for level walking was -0.70 ± 0.24 W kg^{-1} (mean $\pm$ s.e.m) (Wilcoxon Signed-Rank – two-tailed, $n=9$, $z=-22$; $p=0.0078$; 15.9%) at 1.25 m s^{-1}, -0.53 ± 0.22 W kg^{-1} ($n=9$, $z=-18.5$; $p=0.0273$; 9.7%) at 1.5 m s^{-1}, -0.66 ± 0.26 W kg^{-1} ($n=7$, $z=-12$; $p=0.0469$; 8.9%) at 1.75 m s^{-1}, and -0.74 ± 0.32 W kg^{-1} ($n=9$, $z=-19.5$; $p=0.0195$; 7.8%) at 5.71° (Fig. 3C, Table S3). We measured a slight non-significant reduction of -0.22 ± 0.22 W kg^{-1} ($n=9$, $z=-5$; $p=0.5859$; 4.3%) at 1.0 m s^{-1}. We calculated the efficiency of the exosuit force application (metabolic reduction per unit of applied peak torque [W N^{-1} m^{-1}]) by dividing the metabolic reduction [W kg^{-1}] by peak applied torque [N m kg^{-1}]. Compared to other assistance strategies reported in literature (*38–41*, *43*, *44*), the MBA profile was also more efficient at reducing metabolic demand (Fig. 3E).

Effects of MBA Profile on Biomechanics.

We evaluated the biomechanics of the ankle comparing the MBA profile to the NO-DEVICE condition in each walking task. Peak plantar flexion angle and velocity increased significantly for

all walking tasks with MBA. Peak ankle dorsiflexion angle did not significantly change (Fig. S3, Table S2).

180   Peak net (Bio + Exo) ankle moment did not change significantly in any of walking tasks (Fig. 3A, Fig. S2, Fig. S3, Table S2). Peak biological component of ankle moment was reduced by 2.8% (two-tailed paired t-test; $p=0.1698$), 6.1% ($p=0.0407$), 10.7% ($p=0.0033$), 10.2% ($n=6$, $p=0.0385$), and 15.6% ($p<0.0001$) for 1.0, 1.25, 1.5, 1.75 m s^{-1}, and 5.71° (Fig. S2, Fig. S3, Table S2). Peak biological positive power increased by 18.7% ($p=0.0078$), 26.5% ($p=0.0117$), 30.2% ($p=0.0039$), 36.2% ($n=6$, $p=0.0313$), and 17.5% ($p=0.0391$) (Fig. S3, Table S2).

Average soleus activation during mid-late stance (20% stride to peak ankle torque) significantly decreased by 4.6% (two-tailed paired t-test; $p=0.0463$), 7.18% ($p=0.0449$), 6.6% ($p=0.0490$), 8.5% ($p=0.0371$), 9.2% ($p=0.0493$) for 1.0, 1.25, 1.5, 1.75 m s^{-1}, and 5.71° (Fig. S3, Table S4). Peak soleus activation during stance decreased for the same conditions by 7.6%, 8.7%, 7.7%, 190   7.4%, and 7.7% but the changes were not significant. TA activation did not increase with exosuit assistance, and instead significantly decreased in the 1.25 m s^{-1} condition ($n=9$, Wilcoxon Signed-Rank – two-tailed; $p=0.0117$).

Evaluation of MBA Profile Against Alternative Assistance Strategies.

The four assistance profiles - MBA, Muscle Activation (EMG), Joint Power (POW), and Fixed (FXD) - were evaluated for walking at 1.0, 1.25, 1.75 m s^{-1}, and 5.71° (Fig. 4A). We removed the 1.5 m s^{-1} task to maintain the range of tasks while keeping a reasonable session length. On average, across the four tasks, the metabolic demand with MBA was lower than with FXD, POW, and EMG profiles by 0.28 ± 0.15, 0.26 ± 0.15, and 1.09 ± 0.36 W kg^{-1} (mean $\pm$ std) (Fig. 4B). The 200   peak applied force for the POW and EMG profiles were set to the peaks of the MBA profiles, which were 170 ± 14, 229 ± 21, 329 ± 13, and 335 ± 16 N for 1.0, 1.25, 1.75 m s^{-1}, and 5.71°, to normalize the assistance levels. The peak applied force for the FXD profile was fixed based on participant body mass per the approach in (*15, 37*), and was 430 ± 20 N across the conditions. Across the walking tasks, the metabolic benefit for the given level of torque was higher with MBA compared to FXD, EMG, and POW (Fig. 4C).

Evaluating the Effects of MBA Profile on Muscle Mechanics.

To further understand the muscle-level response, we performed a single-participant study where we collected B-mode US images of the soleus during walking with and without MBA exosuit 210   across 4 walking tasks. Our results suggest that the MBA profile resulted in a decrease in the velocity of concentric contraction towards isometric contraction during mid-stance (Fig. S4).

Proof-of-Concept: Feasibility of Online Assistance Generation in Overground Walking.

As a proof-of-concept for real-world use, we demonstrated the feasibility of online adaptive assistance (*i.e.* capture US data, process it, and generate a profile) in a mobile version for variable-speed, overground outdoor walking (Supp Text, Fig. S5, Fig. S6, Movie S1).

DISCUSSION

220   We have demonstrated that individualized assistance profiles derived directly from measured
soleus muscle dynamics can reduce metabolic demand across a range of relevant walking tasks.
While most other studies have tuned and tested for a single walking task, the generalizable MBA
approach achieved significant metabolic reductions for three level walking speeds (1.25, 1.5, and
1.75 m s^{-1}) and inclined walking (5.71° at 1.25 m s^{-1}) (Fig. 3D) (*45*). Furthermore, the MBA
approach achieved these benefits with relatively low applied force (Fig. 3E, Fig. S7).

These reductions in metabolic energy demand were likely partially due to the reduction in soleus
activation during mid-late stance (Fig. S3, Table S4). Furthermore, our data showed no increase
in antagonist TA co-contraction when assistance was applied, which suggests that the MBA
approach may have enabled a more 'natural' operation in which users did not fight the assistance.
230   TA activity can also help explain the benefit (or lack of benefit) from different levels of assistance
at multiple walking speeds (*46*). Participants also significantly increased biological positive ankle
power when assistance was applied (Fig. S3, Table S2). Although we cannot say from this study,
the increase in ankle power may have provided a metabolic benefit by offloading more proximal
muscles such as the hip flexors/extensors (*44, 47, 48*).

We also aimed to understand the effects of MBA on muscle dynamics. In mid-stance, the MBA
profile was likely successful at minimizing the disruption of well-tuned isometric/eccentric
contraction. We measured minimal change in ankle dorsiflexion during this period of the gait
cycle (Fig. S3) which can be an indicator of trained (*i.e.* effective) exoskeleton use (*49*). Prior
studies have shown that exoskeletons for plantar flexion assistance can result in decreased
240   dorsiflexion angle, which may lead to decreased MT length and reduced tendon stretch (*50*).
Furthermore, in the single-participant study, we measured little to no shift into eccentric
contraction velocity, which supports the prediction that tendon energy storage mechanics will be
maintained with MBA (Fig. S4). Conversely, in late stance, the MBA profile may not have fully
achieved the design goal of completely offsetting soleus positive power. Because ankle
velocity/power increased, we expect that muscle velocity did not decrease when assistance was
applied (Fig. S3, Table S2).

Since the MBA strategy was derived from the user's measured muscle mechanics, the assistance
profiles changed in sync with the user's muscle mechanics as the walking task changed. The
trends in the timing and magnitude of the generated force profiles indicate that our method was
250   able to capture the changes related to the increased muscle force/work demands for faster (*26, 33*)
and inclined walking (*32, 34*) (Supp Text). Although the MBA profile is difficult to parameterize
because each time point is uniquely defined using measured muscle velocity, for deeper analysis
we focused on characterizing the assistance onset timing and peak magnitude, both important and
commonly defined parameters for ankle devices (*15*). Other control parameters (*e.g.* peak timing
and offset timing) have also been used for profile generation (*15*) but were not the primary
parameters of interest for this work.

The onset of force development for the MBA profiles (Fig. 3A, Fig. S2, Table S1) generally fall
into what seems to be an important time slot between the early onset times (~10%) associated
with torque (*51*) and soleus EMG (*23*) profiles, and the later onset times (~45% at 1.25 and 1.5 m
260   s^{-1}) associated with joint positive power used in other studies (*18, 19, 21*). The approaches that
assisted earlier in the gait cycle (or assist too much in early-mid stance) often resulted in

increased total ankle moment (*23*, *43*, *50*) and may have disrupted normal tuned MT dynamics by unloading the energy that was stored in the tendon while the muscle was still isometric (0% to (a) in Fig. 1A). That additional force then needed to be made up in the latter portion of the gait cycle by increasing muscle contraction, delivering high levels of assistance, or directly or indirectly assisting muscles other than soleus (*e.g.* hip flexors) (*20*). In our additional study comparing MBA to EMG-based assistance, the EMG profile timing was earlier than MBA and the MBA profile resulted in lower metabolic demand for all walking tasks (Fig. 4B). Compared to devices that target ankle power, the onset of assistance from our device tended to be earlier. By the time the ankle is producing positive power, the underlying muscle has likely already begun producing positive power. As such, previous approaches may have missed an opportunity to assist the muscle during the early regions of concentric contraction ((a) to (b) in Fig. 1A). In our additional study comparing MBA to a power-based profile (POW), the onset of MBA was earlier than POW, and MBA had better metabolic reductions for all walking tasks (Fig. 4B). As speed and incline increased, the difference in timing between the onset of muscle contraction and joint positive power increased (Fig. 3A, Fig. S2, Fig. S3, Table S1), which suggests the importance of measuring and calculating muscle mechanics to adjust assistance as tasks change.

By tailoring assistance to measured MT dynamics from the individual, the MBA profiles can be highly effective at reducing metabolic demand without the need to apply high forces. Compared to the 0.23 N m kg^{-1} average assistance with MBA, other recent ankle devices applied assistance in the range of 0.39-0.75 N m kg^{-1} at 1.25 m s^{-1} (*15*, *37*, *38*, *40*) (Fig. S7). We directly demonstrated this assistance efficiency in our additional study by comparing MBA against a fixed profile (FXD) that has been proven to be effective at 1.25 m s^{-1} but applies a higher, fixed level of assistance across walking tasks (Fig. 4C) (*15*, *37*). The MBA profile resulted in better metabolic benefit while delivering lower levels of assistance (Fig. 3E). We also showed that too much assistance was detrimental at slow walking speeds, which further suggests that applied assistance may be better informed by muscle mechanics than joint mechanics. Whether a 'task-tuned' FXD profile (*i.e.* not individualized) would perform as well as the MBA profile was unclear as we cannot completely distinguish what portions of the metabolic benefit were from the individualization versus the general characteristics of the profile. We did not try to develop a generic profile for any of the walking tasks due to the large variability in MBA profiles across users. Some of these questions may also be addressed by other studies (*52*).

This ability to achieve metabolic benefit with relatively low forces has implications for exosuit design for long-term, real-world use by allowing for smaller and lighter power sources and actuators, which in turn further decreases loading while increasing comfort. In a proof-of-concept real-world evaluation, we demonstrated online adaptive assistance in a mobile version for variable-speed, overground outdoor walking (Supp Text, Fig. S5, Fig. S67, Movie S1). Unlike HIL optimization, the assistance profile can be generated with only a few seconds of walking data, making rapid individualization of assistance possible in a wide range of walking scenarios. Combined with the relatively low force requirements, this MBA approach opens up the possibility of real-world application to small mobile devices that are comfortable and work synergistically with the user.

The design goal of the MBA approach was to, at least partially, replace the force produced by the muscle during concentric contraction with exosuit assistance and still allow individuals to walk 'normally'. Thus, when designing the approach for the MBA profiles, we intentionally derived the assistance profile from the unassisted muscle dynamics. Inherent in this approach was the

assumption that as individuals become proficient with the device, they will attempt to walk with joint dynamics that are similar to their normal dynamics (*49*). Additionally, we assumed that the muscle dynamics of the individuals would be similar between testing sessions. The alternative would be to measure muscle dynamics while assistance is applied. In this case, even if joint dynamics were unchanged as suggested during mid-stance in our study (Fig. S3), the underlying muscle-tendon dynamics would likely be in an altered state (*50*, *53*). Here, we focused on developing a technique that enabled a reasonably accurate estimate of soleus concentric contraction that could then be applied to developing assistance profiles.

Given the complexity of the plantar flexor MTs, numerous simplifications were employed in our development of the MBA exosuit profile. Our goal in this work was to develop a simple and robust method for estimating the force needed to at least partially offset the shortening of the bulk muscle. We briefly discuss this here but provide additional detail on the justification of assumptions/simplifications and their implications in the Supplementary Text. The soleus MT and the interaction of the soleus with the tendon and two parallel gastrocnemius muscles that make up the triceps surae muscle group are complex (*54*, *55*). The free tendon of the Achilles tendon becomes the aponeurosis as it encapsulates and extends along the length of the muscle (*56*). The displacement of the muscle depends upon the location, and the displacement that is measured more proximally is likely greater than the displacement more towards the ankle (free tendon) (*57*). We picked a location over the medial gastrocnemius (MG) because the soleus MT junction is very distal and difficult to measure (particularly with boots) and the location over the MG provided a stable anchor point. The MBA method additionally assumed that the tendon interacted purely in-series with the soleus muscle, a simplification that has been recommended and used in prior models (*58*, *59*). We assumed a constant soleus moment arm similar to prior work modeling the soleus-Achilles tendon MT (*59*). However, in vivo experiments during walking have found that while 41mm is close to the average moment arm throughout the gait cycle, there can be 1-2mm of variation during the mid-late stance phase (*72*). This variation is small and may lead to errors of 2-5% in the generated force profiles.

We assumed that ankle dorsiflexion minimally affected the measurement of concentric contraction. This assumption may have led to underestimation of force produced by the muscle during concentric contraction as dorsiflexion lengthens the MT. During the late-stance phase, due to the rapid movement of the joint and MT, our estimates of muscle contraction were likely less certain. We assumed that muscle contraction velocity was constant during the push-off phase, an approach that is supported by other work which shows a somewhat linear change in muscle length during late stance (*60*).

There are additional limitations related to the metabolic results. We acknowledge that the MBA profile may not be the *best* assistance for maximizing whole-body metabolic demand. The MBA profile in this article was designed to target a single muscle/joint and thus does not consider the coordination between joints and muscles. For comparison, HIL optimization often targets whole-body metabolic optimization and may capture some of the interactions across multiple muscles or joints. However, as very few studies are conducted at different walking tasks (*46*, *61*), apart from the additional two-participant study in this article, we do not have a good comparison of MBA against other approaches for a range of speeds and inclines.

In this article, we have demonstrated how users' measured muscle dynamics can be used to develop exosuit assistance profiles that are tailored to the individual and adaptive to dynamic

walking tasks. By tuning the assistance to the individuals' muscle mechanics, our MBA strategy provided metabolic benefit in multiple walking tasks using relatively low forces. Thus, the MBA strategy is both effective and efficient. Based on the MBA principles presented in this article, future work may be able to improve estimation methods and closed-loop controllers to enable real-time dynamic control for real-world tasks.

MATERIALS AND METHODS

360

Participants

Nine healthy adults (n=9, 3F 6M; age = 29.1 ± 4.04 yrs (mean ± std); mass = 67.9 ± 12.9 kg; height = 1.71 ± 0.07 m) participated in the study. All participants reported no previous history of musculoskeletal injury or diseases, and all participants provided written informed consent prior to their participation. The study was approved by the Harvard Longwood Medical Area Institutional Review Board, and all methods were carried out in accordance with the approved study protocol.

Experimental Procedure and Study Design

370

Overview: All participants attended three experimental visits: a baseline biomechanics assessment, a training visit, and a testing visit. In brief, in the first visit, participants walked without wearing a device while we measured their baseline biomechanics, including muscle mechanics. These data were used to develop user-specific muscle-based assistance profiles for the different walking tasks which were then applied back to the participant in the second (training) and the third (testing) visits.

Visit 1 - Baseline Biomechanics Assessment: In the first visit, each participant walked on a treadmill at six different walking tasks: five level-ground speeds of 0.75, 1.00, 1.25, 1.5, and 1.75 m s^{-1} and one 5.71° (10%) grade at 1.25 m s^{-1}. Participants walked for 2 minutes for each task while lower-limb segment motions were measured using a motion capture system (Qualisys,

380 Gothenburg, Sweden; 120 Hz) and three-dimensional ground reaction forces (GRF) were measured by an instrumented treadmill (Bertec, Columbus, OH, USA; 1200 Hz). Surface electromyography (EMG) (Delsys, Natick, MA, USA; 1200 Hz) captured muscle activation of the soleus and tibialis anterior. A low-profile ultrasound (US) transducer (MicrUs; Telemed, Vilnius, Lithuania; 113 Hz) attached on the left leg over the medial gastrocnemius captured brightness-mode (B-mode) US images of the medial gastrocnemius and soleus. Participants wore the same shoes during the baseline collection as in the later visits to maintain similar loading conditions. Data from the last 30-seconds of 0.75 m s^{-1} walking were used to estimate Achilles tendon quasi-stiffness as outlined in *Estimation of Achilles Tendon Quasi-Stiffness*, and from the remaining walking conditions to develop the user-specific force profiles for different walking tasks as

390 outlined in ***B-mode Ultrasound-Derived Assistance Profile Generation***.

Visit 2 – Training: In the second session, each participant walked for the latter five tasks (1.00, 1.25, 1.5, and 1.75 m s^{-1}; 5.71°) while wearing an active ankle exosuit applying their customized assistance profiles. At the beginning of each task, the participants underwent a procedure for setting the maximum cable retraction limit to prevent over-rotation at ankle joints (see ***Soft***

Exosuit: Control Approach for details). Then, the participants walked for 5-10 minutes for each task (5 minutes for 1.75 m s^{-1} and 5.71°, 10 minutes for the rest) and experienced walking with the active exosuit using the customized assistance profiles. While walking, the participants were instructed to try to conform to the external assistance and to try not to resist it. For the training session, no measurements were collected.

400   *Visit 3 – Testing:* In the third session, each participant again walked on a treadmill for the same five walking tasks, once while wearing the active exosuit with the muscle-based assistance profiles (MBA) and once without the exosuit (NO-DEVICE). To minimize the sequence effect, the NO-DEVICE conditions were tested first for half the participants and MBA was tested first for the other half. Within the MBA (or NO-DEVICE) grouping, the order of tasks was not randomized. The order was always 1.00, 1.25, 1.5, 5.71°, and 1.75 m s^{-1}. We did this to minimize the potential for fatigue to affect measurements at the slower speeds, and we determined it suitable because different speed/incline tasks were not directly compared with each other (*i.e.* active assistance at 1.0 m s^{-1} was not compared with 1.25 m s^{-1}). While walking for 5 minutes in each walking task and suit condition, we measured the metabolic cost of walking by portable
410   indirect calorimetry (K5; COSMED, Rome, Italy), tibialis anterior (TA) and soleus (SOL) muscle activity with EMG (2040 Hz), and lower-limb segment motions and GRFs. We were concerned about participant comfort biasing metabolic measurements and decided to minimize the placement of sensors underneath or near the textile components of the exosuit. Hence, we did not collect EMG data from the gastrocnemius, and similarly, did not collect ultrasound during the active exosuit conditions in the main study.

B-mode Ultrasound-Derived Assistance Profile Generation

The output of the muscle-based assistance process was an estimate of how much additional force the soleus muscle contributed to the muscle-tendon force by concentrically contracting. Our
420   approach calculates the additional soleus force by estimating the stretch the soleus contraction imparts on the in-series AT and then multiplying by the estimated tendon quasi-stiffness (Eq. 1) (Fig. S1).

$$F_{SOL\_Conc} = \Delta L_{SOL/AT} * k_{AT} * rPCSA_{SOL} \tag{1}$$

While the equation is quite simple, the challenge lies in the inability to easily measure muscle state and tendon physiological properties. In our approach, to calculate the additional stretch the soleus contraction imparts on the in-series AT by shortening ($\Delta L_{SOL/AT}$) for each individual and walking task, we measured the soleus contraction velocity and integrated it to estimate the AT stretch. Furthermore, we estimated the AT quasi-stiffness (k_{AT}) for each individual and scaled the resultant force to the approximate contribution of the soleus relative to the plantar flexors (
430   $rPCSA_{SOL} = 0.54$) (*36*). Many assumptions and simplifications are built into this approach (see Discussion). Our focus was on developing a technique that enabled a reasonably accurate estimate of soleus concentric contraction that could then be applied to developing assistance profiles.

Direct measurements of muscle kinematics: In the first session, we securely attached a low-profile US transducer over the left medial gastrocnemius (MG) which gave a view of both the MG and the underlying soleus (*50, 62*). We assumed that MT dynamics would be similar across both legs

based on prior work studying the soleus across walking speeds (*33*). With the participant walking on the treadmill, for each speed and incline we recorded approximately 10 seconds of continuous B-mode US images of the soleus muscle at ~113 Hz during the last 30 seconds of the trial. The US frames were synced with the motion capture and GRF data.

440   *Estimation of soleus contraction velocity and estimation of Achilles Tendon stretch:* In postprocessing, we used a custom MATLAB (Mathworks, Natick, MA, USA) optical flow algorithm to calculate the soleus velocity that was parallel with the soleus superficial aponeurosis from the continuous sequence of US images (*62*). The soleus velocity was segmented into individual strides based on GRF heel-strike timestamps to obtain an average velocity profile. We integrated the positive (*i.e.* shortening) component of the soleus velocity (Vel_{SOL}^{+}) over the mid-late stance period based on the intention for assistance to increase over the gait cycle and to provide stability to the assistance profile. To calculate the length change of the muscle during the dorsiflexion phase ($\Delta L_{SOL/AT}(t)|_{DF}$), we integrated the measured velocity beginning at 20% gait cycle (*i.e.* $\Delta L_{SOL/AT}(0.2)=0$) up to the transition to ankle plantar flexion (PF) at $t*$ (Eqs. 2, 3).

450   During mid-stance, the ankle is slowly dorsiflexing and elongating the MT. This tends to stretch the muscle and create distal displacement of the muscle. Thus, we assumed that any proximal displacement of the muscle during this intermediate time region is not from joint rotation. Rather, any proximal displacement in this region we take to be from concentric contraction. In the PF phase, because the measured soleus velocity was heavily affected by rapid ankle plantar flexion, we set the velocity to the measured velocity at the transition to PF (*i.e.* $Vel_{SOL}^{+}(t)|_{t\geq t*}=Vel_{SOL}^{+}(t*)$). This approach is supported by other work which shows a somewhat linear change in muscle length during late stance (*60*).

$$t* = \underset{t}{\mathrm{argmin}}\left\{Vel_{ANK}(t) > 0 \,\&\, t > 0.2\right\} \tag{2}$$

$$\Delta L_{SOL/AT}(t) = \int_{\substack{\text{mid-late}\\\text{stance}}} Vel_{SOL}^{+}(t)\cdot dt$$

$$\approx \begin{cases} \int_{0.2}^{t} Vel_{SOL}^{+}(t)\cdot dt & (0.2 \leq t < t*) \\ \int_{0.2}^{t*} Vel_{SOL}^{+}(t)\cdot dt + \int_{t*}^{t} Vel_{SOL}^{+}(t*)\cdot dt & (t* \leq t < TO) \end{cases} \tag{3}$$

460   We then combined the two phases sequentially to estimate the length change of the soleus muscle due to concentric contraction throughout stance. Because the soleus and AT are in-series, we assumed that the additional AT stretch due to concentric contraction was equal to the length change of the soleus (*i.e.* $\Delta L_{SOL/AT} = -\Delta L_{SOL} = \Delta L_{AT}$).

Estimation of Achilles Tendon Quasi-Stiffness: We estimated the individuals' AT quasi-stiffness (length-tension relationship) (k_{AT}) based on the ankle angle and ankle moment during the mid-late stance while walking slowly (*59*). We assumed that the plantar flexor muscles isometrically contract and do not change their length during this period (*i.e.* the ankle angle change is associated only with the AT length change), the dorsiflexor muscles are not active during this

period (*i.e.* the ankle moment is associated only with the force on the AT), and the AT quasi-
stiffness curve is linear. Thus, we estimated that the ankle's quasi-stiffness during this region was
generated from the AT quasi-stiffness. The AT length change and the force on the AT were
estimated for 35-40% gait cycle, from the ankle angle change and the ankle moment during 0.75
m s^{-1} walking respectively, assuming a constant biological moment arm of the ankle (
$ma_{ANK} = 0.041$ m) (*59*). AT force was estimated by dividing the ankle moment by the assumed
moment arm of the biological ankle ($ma_{ANK} = 0.041$ m) (*59*). We then estimated the AT quasi-
stiffness as the slope of a linear regression line between the estimated AT force and AT length.
The average R^2 of the linear regression was 0.998, confirming the linearity assumption was valid.

Generation of assistance profile: We then multiplied the AT stretch profiles for each participant
by their estimated AT quasi-stiffness (k_{AT}) and $rPCSA_{SOL}$ (Eq. 1) to generate an estimated
biological force generated by the soleus concentric contraction for each task and person (F_{SOL_Conc}
). Finally, we calculated the exosuit force (F_{EXO}) required to generate an equivalent (and thus
offsetting) ankle moment to that generated by the estimated soleus muscle force (F_{SOL_Conc}) by
multiplying by the ratio of the assumed moment arm of the biological ankle ($ma_{ANK} = 0.041$) (*59*)
and exosuit ($ma_{EXO} = 0.10$ m) (Eq. 4).

$$F_{EXO} = F_{SOL\_Conc} * \frac{ma_{ANK}}{ma_{EXO}} \tag{4}$$

By providing an equivalent torque, the goal of this method was to offset only the force produced
by the muscle during concentric contraction in mid-late stance when the MT dynamics become
relatively uneconomical.

Direct Comparison of MBA to other assistance profiles

Our direct comparison of MBA against alternative assistance strategies let us better understand
how the MBA performed relative to other bioinspired approaches. For two individuals (1M, 1F),
we performed a direct head-to-head comparison of the MBA profile to other biological
mechanism-derived strategies and an average profile based on a previous optimization study (*15,
37*) in an additional visit. The four assistance profiles were MBA, Muscle Activation (EMG),
Ankle Positive Power (POW), and a fixed literature reference (FXD). We used the participant's
data from the first biomechanics visit which collected baseline soleus EMG, ankle joint dynamics,
and B-Mode ultrasound of the soleus for walking tasks at 1.0, 1.25, 1.75 m s^{-1}, and 5.71° to
develop the assistance profiles. The baseline soleus EMG envelope and positive ankle power
profiles calculated in each walking task were used as the assistance profiles for EMG and POW
respectively, and thus, each profile was unique to both the user and the walking task. The peak
demanded force for the MBA, EMG, and POW profiles were set to be the same to allow for a fair
comparison across biologically inspired approaches as prior studies have shown that increasing
assistance magnitude can increase metabolic benefit (*20*). For FXD, an averaged profile from a
previous human-in-the-loop optimization study (*15*) was used. This reference has been used in
other ankle assistive device papers (*37*). The peak magnitude of the averaged ankle moment

assistance profile was 0.75 N m kg^{-1} and the profile was scaled by each participant's body weight (60 and 56 kg, respectively) and the moment arm of the exosuit ($ma_{EXO} = 0.10$ m).

On the testing day, each participant walked on a treadmill in the order of 1.00, 1.25, 5.71°, and 1.75 m s^{-1}. We removed the 1.5 m s^{-1} task to maintain the range of tasks and while keeping a reasonable session length. The four assistance profiles were applied at each walking task in randomized order. The participant walked for 5 minutes for each suit condition and walking task, and we measured the metabolic cost of walking with portable indirect calorimetry. A training day was not performed. The two participants had been tested with the MBA profile previously, but because the gap between this and the previous session was 8 months, we determined that training was not a factor.

Soft Exosuit

Apparel components: The soft exosuit was designed to assist ankle plantar flexion during walking (Fig. 3B). The exosuit textile components per leg consisted of an underlying Fabrifoam® liner, a calf wrap, and an arch-shaped rigid plastic shield inserted in between to prevent compression-induced fatigue of the tibialis anterior (TA) muscle. The calf wraps were similar to those previously reported by our group (*18, 63*), but redistributed the compression towards the most superior region of the shank to permit the calf muscles to bulge in a more physiologically relevant manner while walking (*64*).

Hardware implementation: An offboard actuator with two custom motors (Allied Motion Technologies, Amherst, NY, USA) was used to generate assistive forces (*65, 66*). Bowden cables between the posterior calves and heels were used to transmit the forces to the user. An inertial measurement unit (IMU; MTi-3 AHRS; Xsens Technologies, Enschede, Netherlands) on each foot and a load cell (LSB200; Futek Advanced Sensor Technology, Irvine, CA, USA) on each calf wrap were used to track and apply assistance. All components on both legs had a total mass of 0.68 kg.

Control approach: A real-time target machine (Speedgoat, Liebefeld, Switzerland) ran a custom Simulink (MathWorks, Natick, MA, USA) model to drive the motors in the offboard actuator. The high-level controller in the Simulink model was designed to generate the desired force profiles over a gait cycle while not rotating the ankle joints excessively. First, the controller detected heel strikes for each leg using the foot IMU and segmented walking cycles (*21*). Then, the controller ran a PI force control loop cascaded with a current loop to track the desired force profile (*66*). While running the force control loop, the controller also monitored the Bowden cable retraction length and released the cable as soon as the motor reached a participant/task-specific maximum retraction threshold. For this, at the beginning of each active exosuit condition, a handheld controller was used to allow the participant to set the cable retraction threshold as high as possible while ensuring the assistance did not over-rotate their ankles. This approach enabled safe and robust force tracking until the end of push-off.

Data Analysis

Analog GRF data and marker positions were filtered at 10 Hz. For identifying t^* only, we separately filtered marker positions for kinematics at 20 Hz. We performed inverse dynamics

analysis to calculate the left leg total joint moments and powers (Visual 3D; C-Motion, Germantown, MD, USA). Exosuit torque was calculated by multiplying the exosuit force measured by load cells by the exosuit moment arm. Exosuit moment arm was dynamic and calculated for the entire stride as the perpendicular distance between the joint center and line between markers on either end of the exposed inner Bowden cable (boot attachment and calf wrap). The biological contribution to the total ankle joint moment was calculated by subtracting the calculated exosuit torque from the total ankle moment. Joint angles and moments were reported for the sagittal plane. To calculate the EMG linear envelope, the raw EMG was band-pass filtered at 20-450 Hz, rectified, and low-pass filtered at 10 Hz. The amplitude of the EMG envelope for each muscle was normalized to the peak amplitude for that muscle measured across all walking tasks and suit conditions for each participant. For each participant, suit condition, and walking task, the joint mechanics and muscle activation data were segmented by heel strikes, time-normalized, and averaged to generate average time-normalized metrics. For the summary statistics, average data (*e.g.* average moment) was the time-integral of the time series data divided by the time period. Average data for particular phases of a stride were computed as the time-integral over that phase divided by the time elapsed during that gait phase.

Statistics

For net metabolic power, joint dynamics, and EMG, we reported the means and standard errors calculated across participants. The MBA profile was statistically evaluated against NO-DEVICE at each walking task independently (JMP Pro; SAS Institute, Cart, NC, USA). In the evaluation of the effectiveness of the assistance profile, no statistical comparison was made across different walking tasks. For metrics where data were normally distributed, we used a paired t-test to compare MBA to NO-DEVICE ($\alpha = 0.05$). Net metabolic data were not normally distributed, and we applied the Wilcoxon Signed-Rank – two-tailed test ($\alpha = 0.05$). Two individuals were unable to complete fast walking (1.75 m s^{-1}), and we report the actual sample size in the text ($n=7$). Joint mechanics and EMG data were unusable for some other conditions due to noise or treadmill belt crossovers and we report the actual sample size next to the data. No statistical analysis was performed for the additional studies due to the small sample size.

Supplementary Materials

References and Notes

1. R. W. Bohannon, Comfortable and maximum walking speed of adults aged 20-79 years: Reference values and determinants. *Age Ageing*. **26**, 15–19 (1997).
2. M. M. Samson, A. Crowe, P. L. de Vreede, J. A. G. Dessens, S. A. Duursma, H. J. J. Verhaar, Differences in gait parameters at a preferred walking speed in healthy subjects due to age, height and body weight. *Aging Clin. Exp. Res.* **13**, 16-21 (2001).
3. E. Mattsson, U. Evers Larsson, S. Rössner, Is walking for exercise too exhausting for obese women? *Int. J. Obes.* **21**, 380-386 (1997).
4. R. C. Browning, E. A. Baker, J. A. Herron, R. Kram, Effects of obesity and sex on the energetic cost and preferred speed of walking. *J Appl Physiol*. **100**, 390–398 (2006).
5. D. Malatesta, D. Simar, Y. Dauvilliers, R. Candau, F. Borrani, C. Préfaut, C. Caillaud, Energy cost of walking and gait instability in healthy 65- and 80-yr-olds. *J. Appl. Physiol.* **95**, 2248-2256 (2003).
6. R. M. Guimaraes, B. Isaacs, Characteristics of the gait in old people who fall. *Disabil. Rehabil.* **2**, 177-180 (1980).
7. S. L. Patterson, L. W. Forrester, M. M. Rodgers, A. S. Ryan, F. M. Ivey, J. D. Sorkin, R. F. Macko, Determinants of Walking Function After Stroke: Differences by Deficit Severity. *Arch. Phys. Med. Rehabil.* **1**, 115-119 (2007).
8. D. Tan, M. Danoudis, J. McGinley, M. E. Morris, Relationships between motor aspects of gait impairments and activity limitations in people with Parkinson's disease: A systematic review. *Park. Relat. Disord.* **18**, 117-124 (2012).
9. R. L. Knoblauch, M. T. Pietrucha, M. Nitzburg, Field studies of pedestrian walking speed and start-up time. *Transp. Res. Rec.* **1**, 27-38 (1996).
10. R. Rastogi, I. Thaniarasu, S. Chandra, Design Implications of Walking Speed for Pedestrian Facilities. *J. Transp. Eng.* **137**, 687-696 (2011).
11. F. A. Panizzolo, S. Lee, T. Miyatake, D. M. Rossi, C. Siviy, J. Speeckaert, I. Galiana, C. J. Walsh, Lower limb biomechanical analysis during an unanticipated step on a bump reveals specific adaptations of walking on uneven terrains. *J Exp Biol*. **220**, 4169–4176 (2017).
12. C. M. Wall-Scheffler, Sex Differences in Incline-Walking among Humans. *Integr. Comp. Biol.* **55**, 1155-1165 (2015).

13. D. J. Farris, G. S. Sawicki, The mechanics and energetics of human walking and running: a joint level perspective. *J R Soc Interface*. **9**, 110–118 (2012).

14. J. R. Montgomery, A. M. Grabowski, The contributions of ankle, knee and hip joint work to individual leg work change during uphill and downhill walking over a range of speeds. *R. Soc. Open Sci.* **5**, 180550 (2018).

15. J. Zhang, P. Fiers, K. A. Witte, R. W. Jackson, K. L. Poggensee, C. G. Atkeson, S. H. Collins, Human-in-the-loop optimization of exoskeleton assistance during walking. *Science* **356**, 1280–1284 (2017).

16. Y. Ding, M. Kim, S. Kuindersma, C. J. Walsh, Human-in-the-loop optimization of hip assistance with a soft exosuit during walking. *Sci. Robot.* **3**, eaar5438 (2018).

17. K. A. Witte, P. Fiers, A. L. Sheets-Singer, S. H. Collins, Improving the energy economy of human running with powered and unpowered ankle exoskeleton assistance. *Sci. Robot.* **5** eaay9108 (2020).

18. S. Lee, J. Kim, L. Baker, A. Long, N. Karavas, N. Menard, I. Galiana, C. J. Walsh, Autonomous multi-joint soft exosuit with augmentation-power-based control parameter tuning reduces energy cost of loaded walking. *J Neuroeng Rehabil*. **15**, 66 (2018).

19. L. M. Mooney, E. J. Rouse, H. M. Herr, Autonomous exoskeleton reduces metabolic cost of human walking. *J Neuroeng Rehabil*. **11**, 80 (2014).

20. B. T. Quinlivan, S. Lee, P. Malcolm, D. M. Rossi, M. Grimmer, C. Siviy, N. Karavas, D. Wagner, A. Asbeck, I. Galiana, Assistance magnitude versus metabolic cost reductions for a tethered multiarticular soft exosuit. *Sci. Robot.* **2**, eaah4416 (2017).

21. S. Lee, S. Crea, P. Malcolm, I. Galiana, A. Asbeck, C. Walsh, Controlling negative and positive power at the ankle with a soft exosuit, in *Proc. 33rd IEEE Int. Conf. Robot. Autom.*, 3509-3515 (2016).

22. M. Grimmer, B. T. Quinlivan, S. Lee, P. Malcolm, D. M. Rossi, C. Siviy, C. J. Walsh, Comparison of the human-exosuit interaction using ankle moment and ankle positive power inspired walking assistance. *J. Biomech.* **83**, 76–84 (2019).

23. J. R. Koller, D. A. Jacobs, D. P. Ferris, C. D. Remy, Learning to walk with an adaptive gain proportional myoelectric controller for a robotic ankle exoskeleton. *J. Neuroeng. Rehabil.* **12**, 97 (2015).

24. K. Z. Takahashi, M. D. Lewek, G. S. Sawicki, A neuromechanics-based powered ankle exoskeleton to assist walking post-stroke: a feasibility study. *J. Neuroeng. Rehabil.* **12**, 23 (2015).

25. T. J. Roberts, R. L. Marsh, P. G. Weyand, C. R. Taylor, Muscular force in running turkeys: the economy of minimizing work. *Science.* **275**, 1113–1115 (1997).

26. D. J. Farris, G. S. Sawicki, Human medial gastrocnemius force-velocity behavior shifts with locomotion speed and gait. *Proc Natl Acad Sci U S A*. **109**, 977–982 (2012).

27. M. Ishikawa, P. V Komi, M. J. Grey, V. Lepola, G. P. Bruggemann, Muscle-tendon interaction and elastic energy usage in human walking. *J Appl Physiol*. **99**, 603–608 (2005).

28. R. M. Alexander, Optimum Muscle Design for Oscillatory Movements. *J Theor Biol*. **184**, 253–259 (1997).

29. A. V Hill, The heat of shortening and the dynamic constants of muscle. *Proc. R. Soc. London. Ser. B - Biol. Sci.* **126**, 136–195 (1938).

30. T. W. Ryschon, M. D. Fowler, R. E. Wysong, A.-R. Anthony, R. S. Balaban, Efficiency of human skeletal muscle in vivo: comparison of isometric, concentric, and eccentric muscle action. *J. Appl. Physiol.* **83**, 867–874 (1997).

31. E. M. Arnold, S. R. Hamner, A. Seth, M. Millard, S. L. Delp, How muscle fiber lengths and velocities affect muscle force generation as humans walk and run at different speeds. *J Exp Biol*. **216**, 2150–2160 (2013).

32. N. T. Pickle, A. M. Grabowski, A. G. Auyang, A. K. Silverman, The functional roles of muscles during sloped walking. *J. Biomech.* **49**, 3244–3251 (2016).

33. A. Lai, G. A. Lichtwark, A. G. Schache, Y. C. Lin, N. A. Brown, M. G. Pandy, In vivo behavior of the human soleus muscle with increasing walking and running speeds. *J Appl Physiol*. **118**, 1266–1275 (2015).

34.   G. S. Sawicki, D. P. Ferris, Mechanics and energetics of incline walking with robotic ankle exoskeletons. *J Exp Biol*. **212**, 32–41 (2009).

35.   T. J. Roberts, The integrated function of muscles and tendons during locomotion. *Comp. Biochem. Physiol. - A Mol. Integr. Physiol.* **133**, 1087–1099 (2002).

36.   T. Fukunaga, R. R. Roy, F. G. Shellock, J. A. Hodgson, M. K. Day, P. L. Lee, H. Kwong-Fu, V. R. Edgerton, Physiological cross-sectional area of human leg muscles based on magnetic resonance imaging. *J Orthop Res*. **10**, 928–934 (1992).

37.   R. W. Jackson, S. H. Collins, Heuristic-Based Ankle Exoskeleton Control for Co-Adaptive Assistance of Human Locomotion. *IEEE Trans. Neural Syst. Rehabil. Eng.* **10**, 2059-2069 (2019).

38.   G. S. Sawicki, D. P. Ferris, Powered ankle exoskeletons reveal the metabolic cost of plantar flexor mechanical work during walking with longer steps at constant step frequency. *J. Exp. Biol.* **212**, 21–31 (2009).

39.   P. Malcolm, W. Derave, S. Galle, D. De Clercq, A simple exoskeleton that assists plantarflexion can reduce the metabolic cost of human walking. *PLoS One*. **8**, e56137 (2013).

40.   S. Galle, P. Malcolm, S. H. Collins, D. De Clercq, Reducing the metabolic cost of walking with an ankle exoskeleton: interaction between actuation timing and power. *J. Neuroeng. Rehabil.* **14**, 1–16 (2017).

41.   C. Khazoom, C. Veronneau, J. P. L. Bigue, J. Grenier, A. Girard, J. S. Plante, Design and control of a multifunctional ankle exoskeleton powered by magnetorheological actuators to assist walking, jumping, and landing. *IEEE Robot. Autom. Lett.* **4**, 3083-2090 (2019).

42.   L. M. Mooney, E. J. Rouse, H. M. Herr, Autonomous exoskeleton reduces metabolic cost of human walking during load carriage. *J Neuroeng Rehabil*. **11**, 80 (2014).

43.   S. H. Collins, M. B. Wiggin, G. S. Sawicki, Reducing the energy cost of human walking using an unpowered exoskeleton, *Nature*. **522**, 212-215 (2015).

44.   L. M. Mooney, H. M. Herr, Biomechanical walking mechanisms underlying the metabolic reduction caused by an autonomous exoskeleton, *J. Neuroeng. Rehabil.* **13**, 4 (2016).

45.   G. S. Sawicki, O. N. Beck, I. Kang, A. J. Young, The exoskeleton expansion: improving walking and running economy. *J. Neuroeng. Rehabil.* **17**, 25 (2020).

46.   R. W. Nuckols, G. S. Sawicki, Impact of elastic ankle exoskeleton stiffness on neuromechanics and energetics of human walking across multiple speeds. *J. Neuroeng. Rehabil.* **17**, 75 (2020).

47.   C. L. Lewis, D. Ferris, Walking with increased ankle pushoff decreases hip muscle moments, *J. Biomech.* **41**, 2082-2089 (2008).

48.   S. N. Fickey, M. G. Browne, J. R. Franz, Biomechanical effects of augmented ankle power output during human walking. *J. Exp. Biol.*, **221**, 182113 (2018).

49.   K. E. Gordon, D. P. Ferris, Learning to walk with a robotic ankle exoskeleton. *J Biomech*. **40**, 2636–2644 (2007).

50.   R. W. Nuckols, T. J. M. Dick, O. N. Beck, G. S. Sawicki, Ultrasound imaging links soleus muscle neuromechanics and energetics during human walking with elastic ankle exoskeletons. *Sci. Rep.* **10**, 3604 (2020).

51.   R. W. Jackson, S. H. Collins, An experimental comparison of the relative benefits of work and torque assistance in ankle exoskeletons. *J Appl Physiol*. **119**, 541–557 (2015).

52.   K. L. Poggensee, S. H. Collins, How adaptation, training, and customization contribute to benefits from exoskeleton assistance. *bioRxiv*, in press, doi:10.1101/2021.04.25.440289.

53.   R. W. Jackson, C. L. Dembia, S. L. Delp, S. H. Collins, Muscle-tendon mechanics explain unexpected effects of exoskeleton assistance on metabolic rate during walking. *J Exp Biol*. **220**, 2082–2095 (2017).

54.   T. Finni, J. A. Hodgson, A. M. Lai, V. R. Edgerton, S. Sinha, Mapping of movement in the isometrically contracting human soleus muscle reveals details of its structural and functional complexity. *J. Appl. Physiol.* **95**, 2128–2133 (2003).

55.   J. A. Hodgson, T. Finni, A. M. Lai, V. R. Edgerton, S. Sinha, Influence of structure on the tissue dynamics of the human soleus muscle observed in MRI studies during isometric contractions. *J. Morphol.* **267**, 584–601 (2006).

56. E. Azizi, G. M. Halenda, T. J. Roberts, Mechanical properties of the gastrocnemius aponeurosis in wild turkeys. *Integr. Comp. Biol.* **1**, 51-58 (2009).
57. T. Finni, J. A. Hodgson, A. M. Lai, V. R. Edgerton, S. Sinha, Nonuniform strain of human soleus aponeurosis-tendon complex during submaximal voluntary contractions in vivo. *J. Appl. Physiol.* **2**, 829-837 (2003).
58. F. E. Zajac, Muscle and tendon: properties, models, scaling, and application to biomechanics and motor control. *Crit. Rev. Biomed. Eng.* **17**, 359–411 (1989).
59. G. S. Sawicki, N. S. Khan, A Simple Model to Estimate Plantarflexor Muscle-Tendon Mechanics and Energetics During Walking With Elastic Ankle Exoskeletons. *IEEE Trans Biomed Eng.* **63**, 914–923 (2016).
60. J. Rubenson, N. J. Pires, H. O. Loi, G. J. Pinniger, D. G. Shannon, On the ascent: the soleus operating length is conserved to the ascending limb of the force-length curve across gait mechanics in humans. *J. Exp. Biol.* **215**, 3539–3551 (2012).
61. J. Kim, G. Lee, R. Heimgartner, D. A. Revi, N. Karavas, D. Nathanson, I. Galiana, A. Eckert-Erdheim, P. Murphy, D. Perry, N. Menard, D. K. Choe, P. Malcolm, C. J. Walsh, Reducing the metabolic rate of walking and running with a versatile, portable exosuit. *Science.* **365**, 668-672 (2019).
62. R. W. Nuckols, K. Swaminathan, S. Lee, L. Awad, C. J. Walsh, R. D. Howe, Automated detection of soleus concentric contraction in variable gait conditions for improved exosuit control. in *Proc. IEEE Int. Conf. Robot. Autom.* 4855-4862 (2020).
63. S. Lee, N. Karavas, B. T. Quinlivan, D. LouiseRyan, D. Perry, A. Eckert-Erdheim, P. Murphy, T. G. Goldy, N. Menard, M. Athanassiu, J. Kim, G. Lee, I. Galiana, C. J. Walsh, Autonomous multi-joint soft exosuit for assistance with walking Overground, in *Proc. IEEE Int. Conf. Robot. Autom.* 2812–2819 (2018).
64. E. Azizi, E. L. Brainerd, T. J. Roberts, Variable gearing in pennate muscles. *Proc. Natl. Acad. Sci. U. S. A.* **105**, 1745-1750 (2008).
65. G. Lee, Y. Ding, I. G. Bujanda, N. Karavas, Y. M. Zhou, C. J. Walsh, Improved assistive profile tracking of soft exosuits for walking and jogging with off-board actuation, in *Proc. IEEE/RSJ Int. Conf. on Intelligent Robots and Systems.* 1699–1706 (2017).
66. M. Kim, C. Liu, J. Kim, S. Lee, A. Meguid, C. J. Walsh, S. Kuindersma, Bayesian optimization of soft exosuits using a metabolic estimator stopping process, in *Proc. IEEE Int. Conf. Robot. Autom.* 9173-9179 (2019).
67. G. A. Lichtwark, A. M. Wilson, In vivo mechanical properties of the human Achilles tendon during one-legged hopping. *J Exp Biol.* **208**, 4715–4725 (2005).
68. G. L. Onambele, M. V Narici, C. N. Maganaris, Calf muscle-tendon properties and postural balance in old age. *J Appl Physiol.* **100**, 2048–2056 (2006).
69. K. C. Moisio, D. R. Sumner, S. Shott, D. E. Hurwitz, Normalization of joint moments during gait: a comparison of two techniques. *J. Biomech.* **36**, 599–603 (2003).
70. D. J. Farris, G. A. Lichtwark, UltraTrack: Software for semi-automated tracking of muscle fascicles in sequences of B-mode ultrasound images. *Comput Methods Programs Biomed.* **128**, 111–118 (2016).
71. E. Azizi, T. J. Roberts, Biaxial strain and variable stiffness in aponeuroses. *J. Physiol.* **587**, 4309-4318 (2009).
72. K. Rasske, D. G. Thelen, J. R. Franz, Variation in the human Achilles tendon moment arm during walking. *Comput. Methods Biomech. Biomed. Engin.* **20**, 201–205 (2017).
73. T. J. M. Dick, A. S. Arnold, J. M. Wakeling, Quantifying Achilles tendon force in vivo from ultrasound images. *J. Biomech.* (2016), doi:10.1016/j.jbiomech.2016.07.036.
74. G. A. Lichtwark, A. M. Wilson, Interactions between the human gastrocnemius muscle and the Achilles tendon during incline, level and decline locomotion. *J. Exp. Biol.* **209**, 4379–4388 (2006).
75. N. J. Cronin, B. I. Prilutsky, G. A. Lichtwark, H. Maas, Does ankle joint power reflect type of muscle action of soleus and gastrocnemius during walking in cats and humans? *J. Biomech.* **46**, 1383–1386 (2013).

780   76.   E. M. Arnold, S. R. Ward, R. L. Lieber, S. L. Delp, A model of the lower limb for analysis of human movement. *Ann Biomed Eng*. **38**, 269–279 (2010).

Figure 1: Ankle muscle-tendon mechanics and energetics. **(A)** Example of length change and power of the muscle fascicle, tendon, and MT (ankle joint) for fast walking (figure reproduced from (*26*)). Between heel-strike (0%) and **(1)** the muscle remains approximately isometric/eccentric, the ankle is dorsiflexing which elongates the MT, and the tendon stores mechanical elastic energy. At **(1)**, muscle concentric contraction begins and the muscle produces positive power. Mechanical energy continues to be stored in the tendon. At **(2)**, the ankle begins plantar flexion and produces positive joint (MT) power. Shortly after at **(3)**, the tendon returns the mechanical energy resulting in a burst of positive power at the ankle. **(B).** Isometric and eccentric muscle contractions are more efficient than concentric contractions (data reproduced from (*28*). The MBA profile is

810

820   designed to selectively target the region of concentric contraction (**(1)** to toe-off) where
the muscle is less efficient.
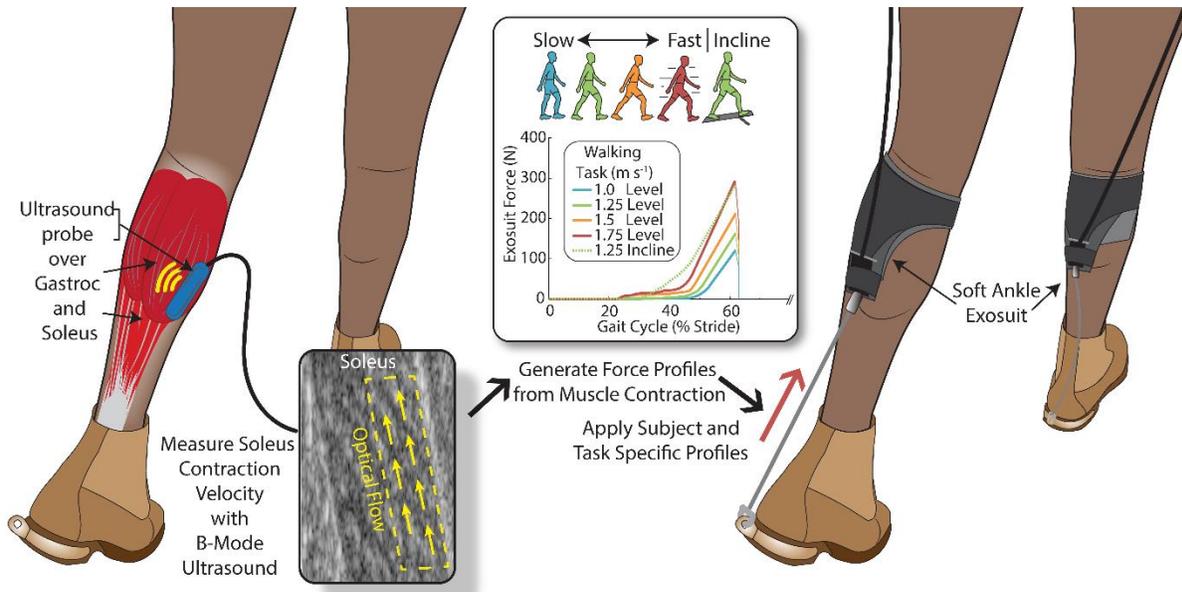
Figure 2: Generation of the muscle-based assistance (MBA) profile from measured soleus dynamics. A low-profile US probe recorded images of the soleus while the participant walked in multiple tasks. We performed offline optical flow image processing to measure the velocity of the muscle concentric contraction. From this velocity profile, we estimated the stretch generated in the tendon and, by multiplying by tendon quasi-stiffness, the force in the tendon generated by muscle concentric contraction. This profile was applied back to the participant through the ankle exosuit to offset the requirement of the soleus to produce positive power and reduce energy use.

830
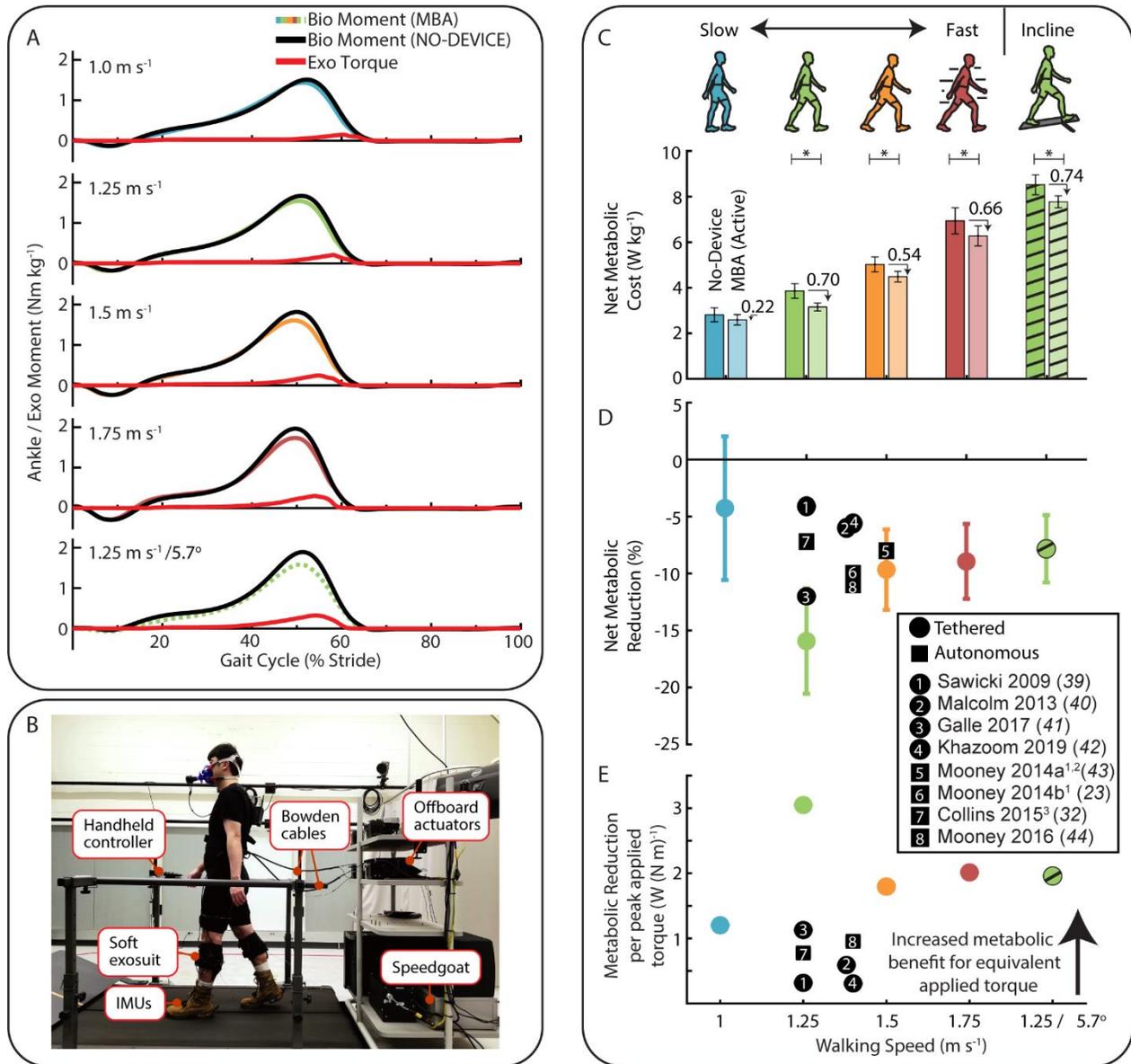
Figure 3: Biomechanical and energetic response to the muscle-based assistance (MBA) ankle exosuit across a range of walking tasks . (A) Group average ankle moment and exosuit torque profiles for each walking task normalized by participant body mass MBA exosuit assistance resulted in lower biological ankle moments. **(B)** Ankle exosuit with offboard actuation for the main study. **(C)** Group average net metabolic energy [W kg^{-1}; mean ± s.e.m] use for each of the walking tasks (p < 0.05). Energy use was lower with the MBA exosuit compared to NO-DEVICE for all except the slowest walking speed. **(D)** Metabolic reduction [%; mean ± s.e.m] for each walking task relative to wearable ankle robots in literature that compared to no-device (19, 38–44). **(E)** The ratio of the metabolic reduction [W kg^{-1}] to the applied ankle assistive torque [N m kg^{-1}]. The MBA ankle exosuit had a higher metabolic benefit for equivalent applied torque. The torques estimated for the MBA profiles were generally lower than those used in other studies (Fig. S7). (Notes: [1]Exoskeleton torque not reported; [2]Walking with load carriage; [3]Passive device; *n*=9 for 1.0 1.25, 1.5 m s^{-1}, and 5.71º; *n*=7 for 1.75 m s^{-1}).

840
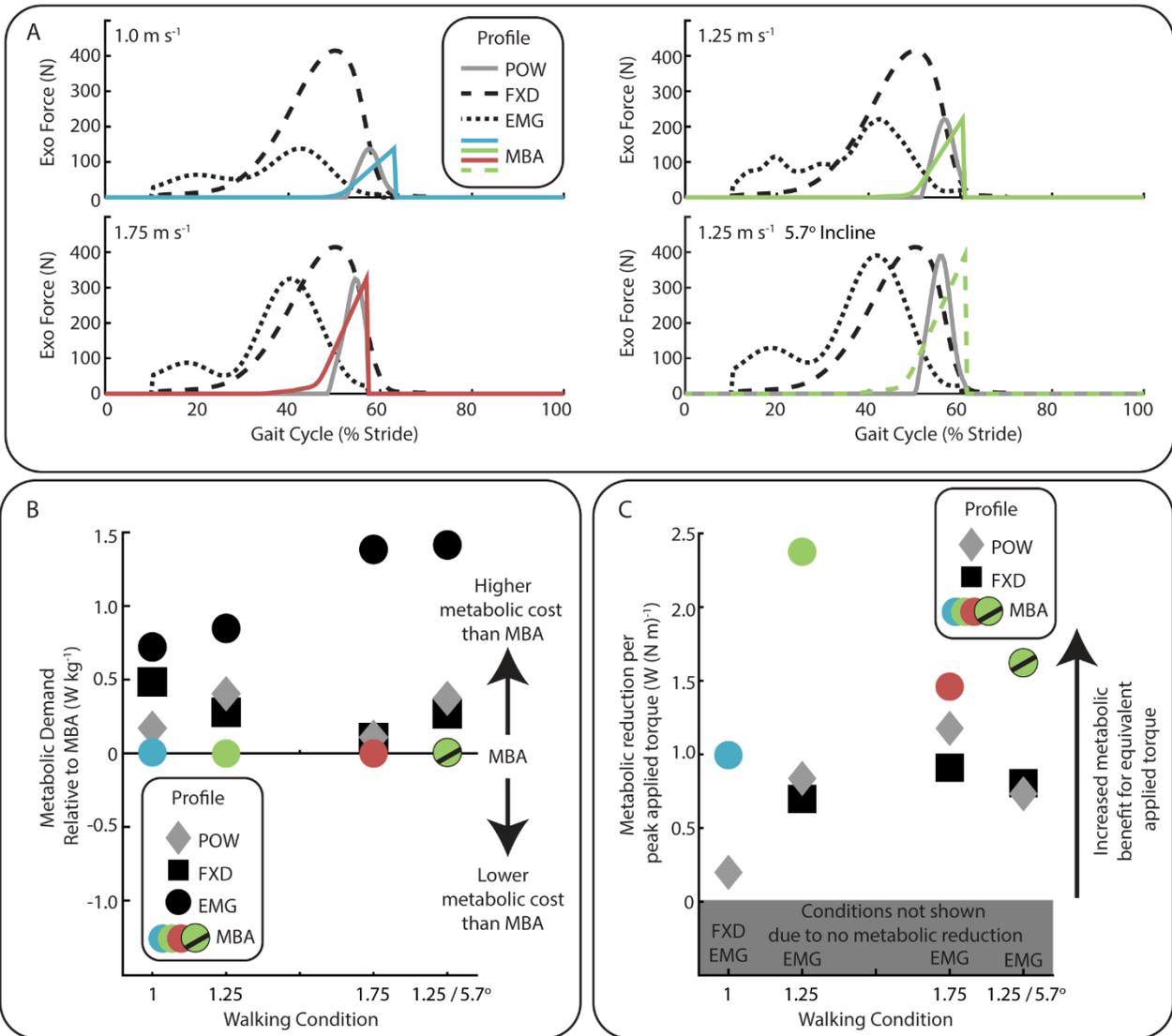
Figure 4: Direct comparison of muscle-based assistance (MBA) to other assistance strategies. For a range of walking speeds and inclines, the effectiveness of the MBA profile was compared to joint power (POW) and muscle activation (EMG) based profiles, and the average profile from a previous optimization study (FXD). **(A)** The three bioinspired profiles (MBA, EMG, POW) were generated from the measured biomechanics of the individual for each walking task while the FXD profile was derived from literature. **(B)** The metabolic energy use for each profile relative to the MBA profile. The MBA profile performed better than the POW, EMG, and FXD profiles at reducing metabolic energy use. **(C)** The ratio of the metabolic reduction [W kg^{-1}] to the applied ankle assistive torque [N m kg^{-1}]. The MBA ankle exosuit had a higher metabolic benefit for equivalent applied torque. (*n*=2)

850

860

Supplementary Text:

Muscle and Joint Response to Variable Walking Tasks:

We analyzed how the joint and the estimated muscle dynamics changed across conditions and participants during unassisted walking. Compared to the muscle, the ankle joint produced relatively similar moments across the walking tasks and participants. Changes in ankle power were more similar to the estimated muscle response across walking speeds (Fig. 3A, Fig. S2, Fig. S3, Table S2). This is likely reflective of increased angular velocity and may suggest that the force generated by concentric contraction of the muscle is primarily directed at increasing joint velocity when modulating walking speed. However, ankle power did not follow the same trend as the muscle for incline walking. The largest disparity between the joint (+13% increase in peak ankle moment and +19% in peak ankle power compared to level) and the estimated muscle force (+92%) happens in incline walking. This is expected as the muscle must produce more work to add energy to the center of mass to overcome gravity, rather than relying upon passive energy storage and return. These data suggest that there may be different neuromuscular strategies that individuals develop depending upon tasks and upon variability in physiologic features such as tendon stiffness (*67*, *68*), that in the end results in more similar response to the external environment at the joint level.

Our data found no correlation between peak MBA exosuit torque (non-mass normalized) and body mass in contrast to the established positive correlation between peak ankle moment (non-mass normalized) and body mass (*69*). Because of this relationship between ankle moment and body mass, assistance profiles are often scaled to the participant body mass (*15*, *20*, *37*, *40*, *51*). However, our data suggest that individual underlying physiology can be complicated and nonintuitive, and that assistance strategies should consider the underlying physiology and task-specific demands at the muscle level.

Details on the estimation of velocity, stretch, tendon quasi-stiffness, and force, and their limitations:

The velocity that we measure is an estimate of the displacement of the muscle against the tendon. This is somewhat analogous to the displacement of the muscle-tendon junction but not identical. This measurement of muscle velocity / stretch is not an estimate of the muscle fascicle velocity or length change. While these values are also interesting, the real-time processing is more involved and prone to tracking error drift (*70*). There is the potential that pennation angle can also change which could affect the bulk muscle length separately from the fascicle length (*64*). However, prior work has suggested that pennation angles do not change substantially in the presence of exoskeleton assistance (*50*). This method additionally assumes that the tendon interacts purely in-series with the soleus muscle, a simplification that has been recommended and used in prior models (*58*, *59*).

The force estimate is performed by multiplying the muscle length change by a tendon quasi-stiffness. The estimated tendon quasi-stiffness is derived for each individual from their walking dynamics at 0.75 m s^{-1}. We chose this speed as it gave the most linear results, the muscle dynamics appeared to remain isometric, and this approach was similar to previous studies (*59*). The average R^2 of the linear regression across participants was 0.998, confirming the linearity assumption was valid. We assumed that the quasi-stiffness was the same regardless of tendon

force. While this may be a true statement for the free tendon, this is not necessarily true along the aponeurosis where the bulging of the muscle can cause the quasi-stiffness to increase (*71*). Most likely the quasi-stiffness increases with faster and inclined walking, but we did not model this. Finally, the conversion from muscle force to exosuit force involved scaling by the ratio of soleus and exosuit moment arms relative to the ankle joint. We assumed a constant soleus moment arm similar to prior work modeling the soleus-Achilles tendon MT (*59*). However, in vivo experiments during walking have found that while 41mm is close to the average moment arm throughout the gait cycle, there can be 1-2mm of variation during the mid-late stance phase (*72*). This variation is small and may lead to errors of 2-5% in the generated force profiles.

Comparisons of velocity, stretch, tendon quasi-stiffness, and force

There have been similar efforts to estimate AT and plantar flexor muscle force using B-mode ultrasound (*73*, *74*), but no study focused on the AT force generated only by concentric contraction and then using it for assistive devices.

The velocity and length change estimated by this approach was similar to reported literature values for muscle fascicle velocity and length change, and the changes induced by increasing speed and incline follow similar trends (*33*, *60*, *75*). The velocity we measured across individuals was 20.8 ± 4.4, 29.2 ± 4.7, 37.4 ± 5.0, 39.4 ± 4.6, 39.2 ± 3.8 mm s^{-1} for 1.0, 1.25, 1.5, 1.75 m s^{-1}, and 5.7° (Fig. S2, Table S1). The change in muscle length up to 60% GC was 2.4 ± 0.5, 4.0 ± 0.7, 6.3 ± 0.9, 8.7 ± 1.2, and 7.9 ± 1.0 mm. Although our estimate of muscle velocity and length change is not a direct measure of the muscle fascicle, a comparison to expected values for the soleus fascicle is useful. A review of fascicle shortening velocity in literature seems to suggest that fascicle velocity remains below an approximate value of ~40 mm s^{-1} during walking and is well below the maximum shortening velocity of the soleus of 262 mm s^{-1} (*59*). As walking speed changes, the change in length of the fascicle across slow, mid, and fast walking is approximately 2%, 12%, and 25% (normalized length) (*33*) which corresponds to approximate length changes of 0.9, 5.3, and 11.0 mm (assuming $l_0 = 44$mm (*76*)). The estimated individual AT quasi-stiffness ranged from 116 to 299 N mm^{-1} (188 ± 67 N mm^{-1}; mean $\pm$ std), which is in line with the values reported in literatures (*59*, *67*).

The estimated force produced by the soleus through concentric contraction was 89.65 ± 16.76, 148.03 ± 20.34, 238.75 ± 26.69, 328.47 ± 28.99, and 295.84 ± 18.38 N for 1.0, 1.25, 1.5, 1.75 m s^{-1}, and 5.7° (Fig. S23, Table S1). Estimate of biological force is well below the maximum force capacity of the soleus ($F_{max/SOL} = 3500$) (*76*) and below the expected force produced from the soleus muscle in walking (Peak F_{SOL} ~=1500N) (*50*). Because we are only estimating the additional contribution though muscle concentric contraction, we should expect that our estimated force is less than the total produced in walking. One potential way to cross-check this estimate of additional force generated is to consider the estimated muscle force (ankle torque) before and after the estimated onset of muscle concentric contraction. For example, from the force in (*50*), for an onset of muscle contraction at 42% of the stride, the muscle had already developed approximately 75% of the force (or 1125 N). The remaining 375N was presumably contributed by muscle concentric contraction and additional strain due to dorsiflexion and was similar in magnitude to the obtained estimated forces in this study.

Proof-of-Concept Study: Mobile ankle exosuit with real-time on-demand MBA profile generation

For one participant, we performed an outdoor walking test to see the feasibility of real-time MBA profile generation with a mobile ankle exosuit. There was one additional visit for this participant. We used the participant's data from the first biomechanics visit to pre-determine the AT quasi-

950 stiffness (k_{AT}) and the PF transition timing. In the testing day, the participant wore a mobile US-exosuit combined system described below and walked over an outdoor closed-loop walkway (approx. 250 m per lap) for multiple laps continuously. At the beginning of each lap, the participant was asked to freely change the walking speed and maintain the new speed until the end of the lap.

System implementation: The mobile US-exosuit combined system consisted of the low-profile US transducer used in the main study, a mobile ankle exosuit, and two laptops inside of a backpack, controlling the US and the exosuit, respectively. The mobile ankle exosuit used the same apparel components and sensors as the main study but was driven by a pair of mobile actuators mounted at the back of the calves. Each actuator (U5; T-Motor, Jiangxi, China) used a
960 miniature rope winch design, which contained a spool of Dyneema rope (Marlow Ropes, Hailsham, UK; 1.8 mm diameter) extending to a pulley attached at the heel. The electronics contained a microprocessor and two motor controllers that were the same as the main study, which were mounted at the waist along with two 3450-mAh Li-Ion smart batteries (RRC Power Solutions, Homburg, Germany). All components on both legs, including apparel, actuators, electronics, and batteries, had a total mass of 2.84 kg. The exosuit laptop and the exosuit microcontroller communicated via Bluetooth to monitor real-time data from the sensors and to command the updated MBA profiles. The two laptops independently ran custom MATLAB scripts and communicated via UDP to exchange information on the updated MBA profiles and the changes in walking speed.

970 **Finite state machine**: During steady-state walking, the exosuit laptop monitored the real-time sensor signals to detect a change in walking speed (State 0: Exosuit steady-state walking and US standby) (Fig. S56). When the exosuit laptop detected a speed change, defined as a change in average cadence greater than 0.05 Hz sustained over three consecutive strides, the laptop sent a stop command to the exosuit and sent a message to the US laptop to start the US image capture. Then the US probe captured B-mode US images for 5 seconds while the exosuit did not apply any assistance (State 1: Exosuit unactuated and US data capture). After capturing, the US laptop sent a message to the exosuit laptop to gradually start the exosuit assistance, and then the exosuit laptop sent a start command to the exosuit. In parallel, the US laptop processed the captured US images into MBA profiles (State 2: US processing and exosuit standby). After processing, the US laptop
980 sent the resultant MBA profile information to the exosuit laptop, and the exosuit laptop commanded the new profile to the exosuit, returning to active exosuit steady-state walking. In case the captured US images were not good enough to generate MBA profiles, the US laptop sent a message to the exosuit laptop to stop the exosuit assistance, and then the exosuit laptop sent a stop command to the exosuit, going back to the US data capture state.
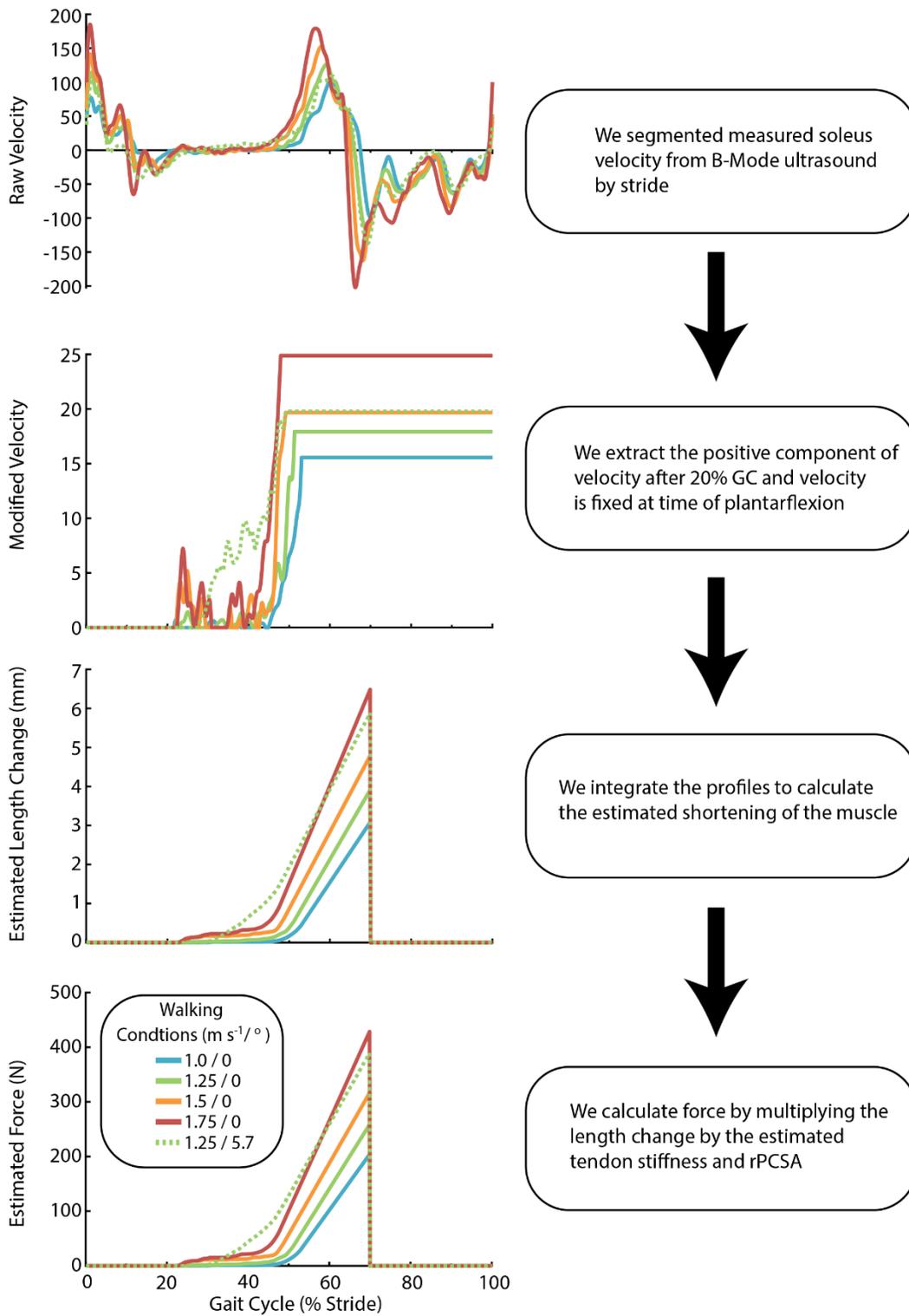
Fig. S1. Profile Generation. Data for one individual shown.

990
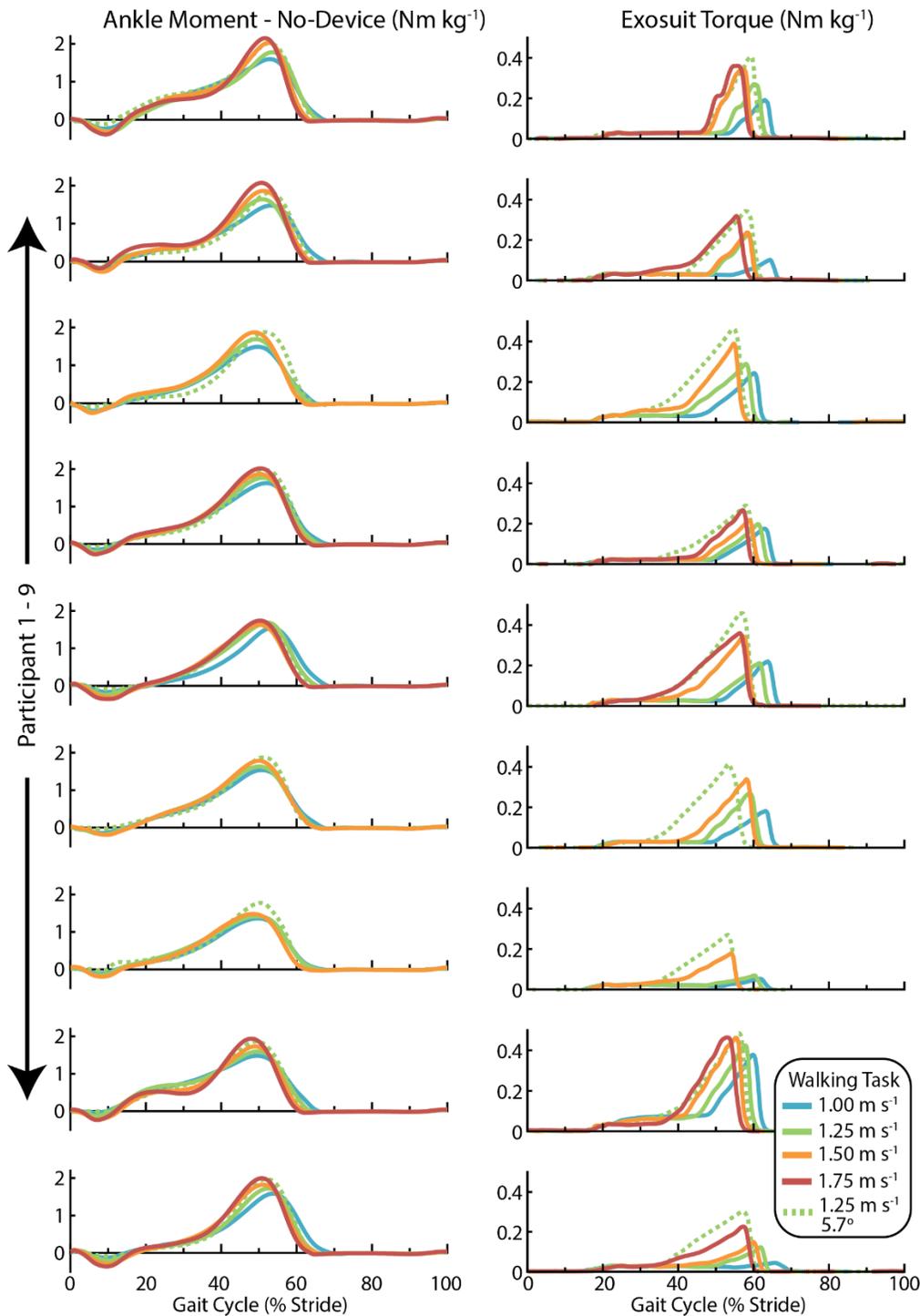
Fig. S2. Ankle moment and applied exosuit torque with the MBA profile for each participant. Two individuals did not complete 1.75 m s^{-1} and the GRF data were unusable (belt crossover) for one individual at 1.75 m s^{-1}.
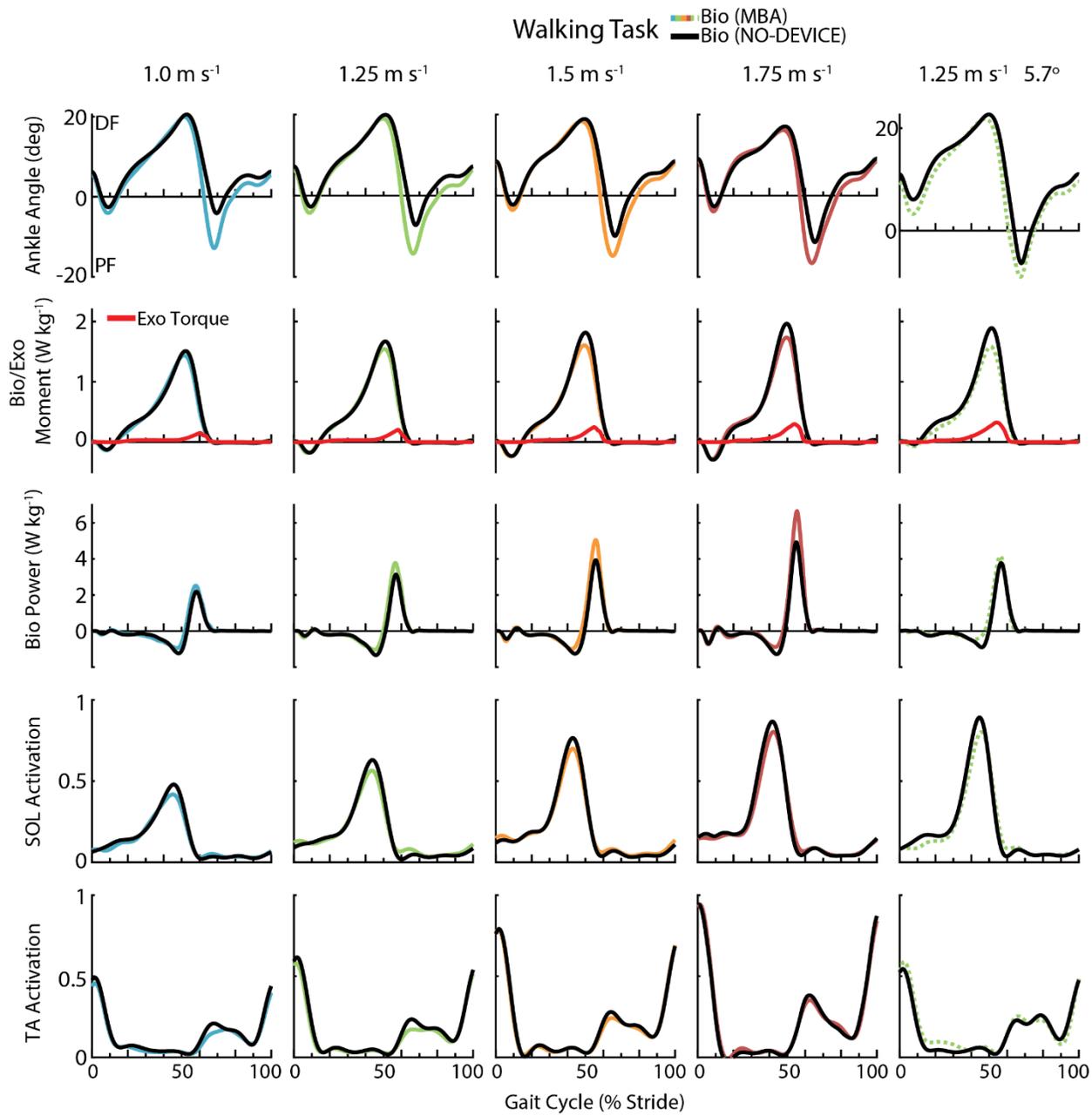
Fig. S3. Ankle Kinematics, Kinetics, and Muscle Activations.
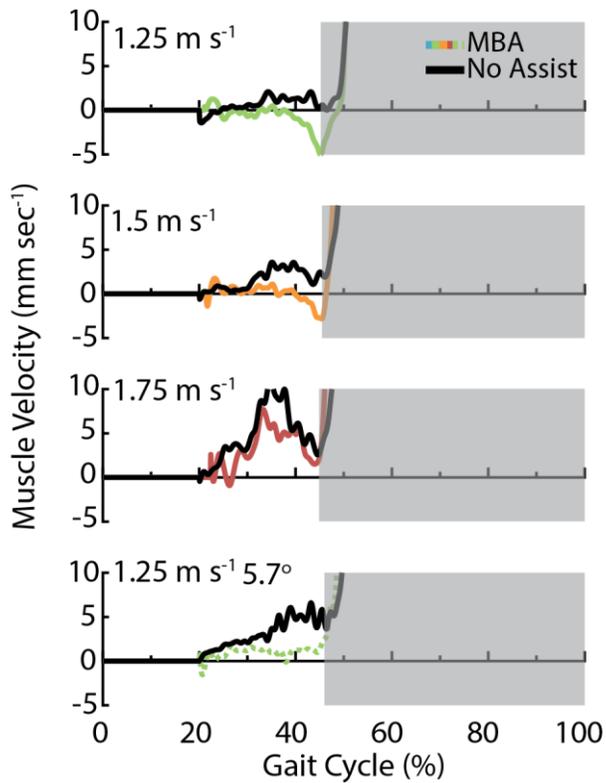
1000   **Fig. S4. Measured muscle velocity with and without MBA assistance.** The gray region represents an area of measurement uncertainty where the ankle begins plantar flexion and high actuator force may cause movement in the probe.
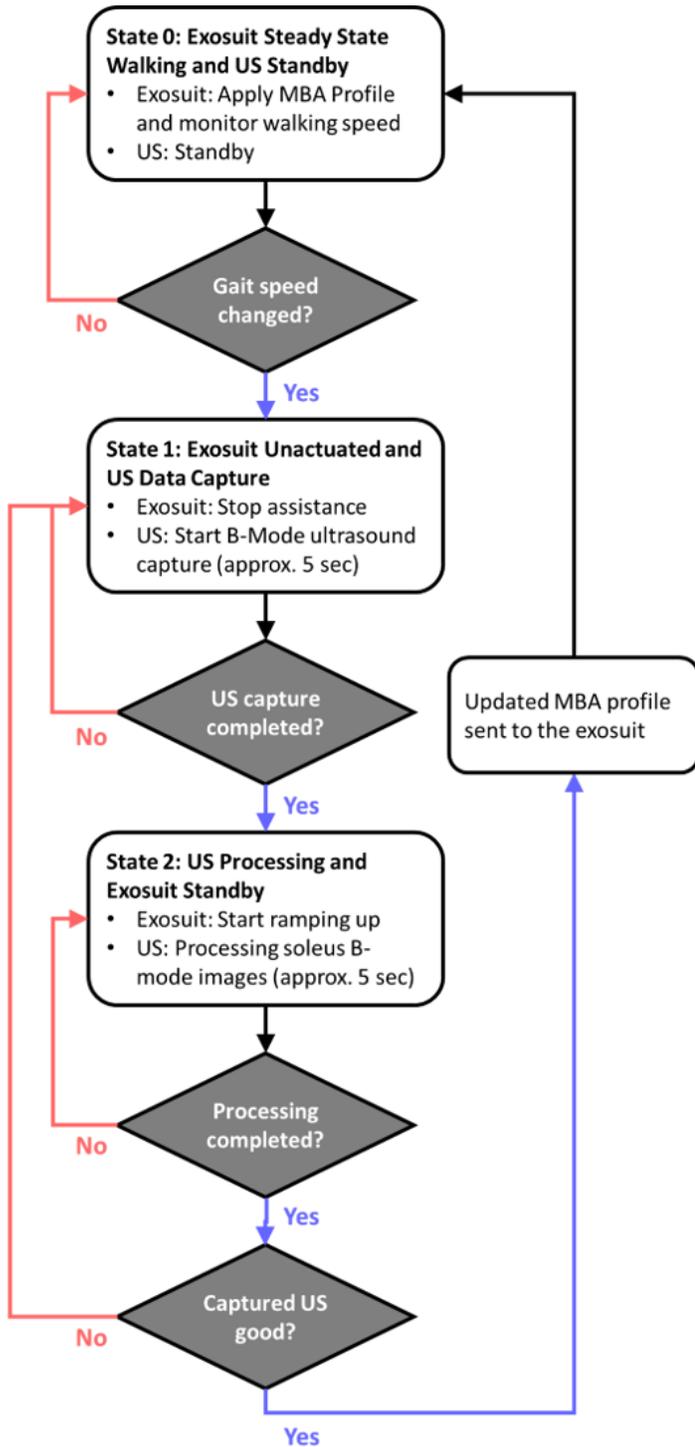
Fig. S5. Finite State Machine diagram for real-time on-demand MBA profile generation.
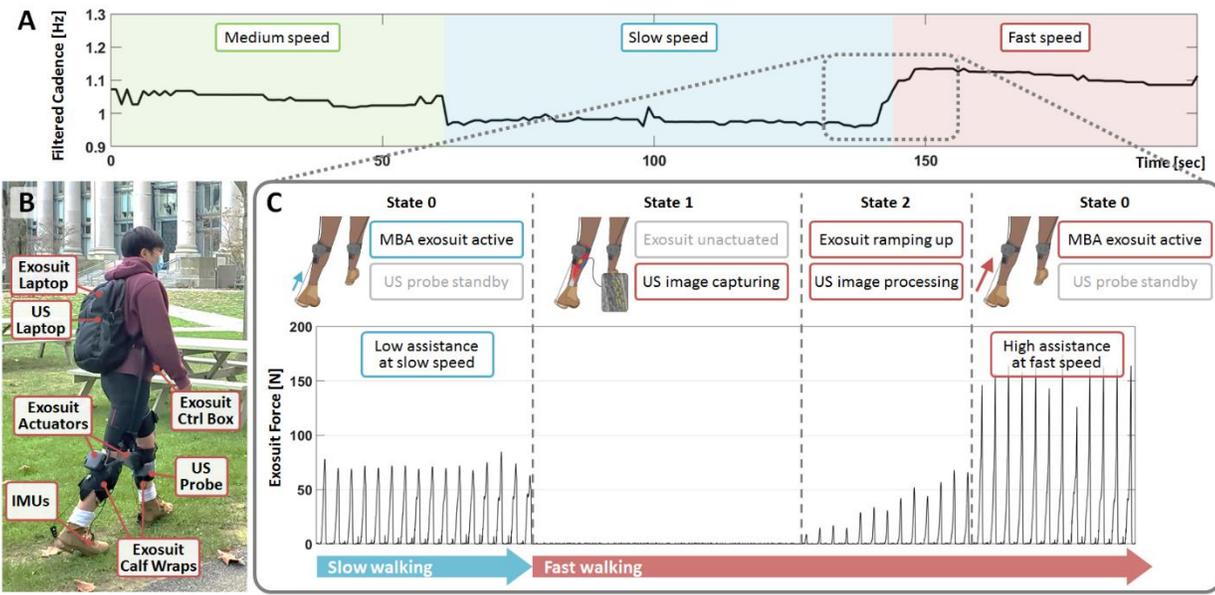
Fig. S6. Outdoor online testing of MBA profile generation with a mobile ankle exosuit.

1010
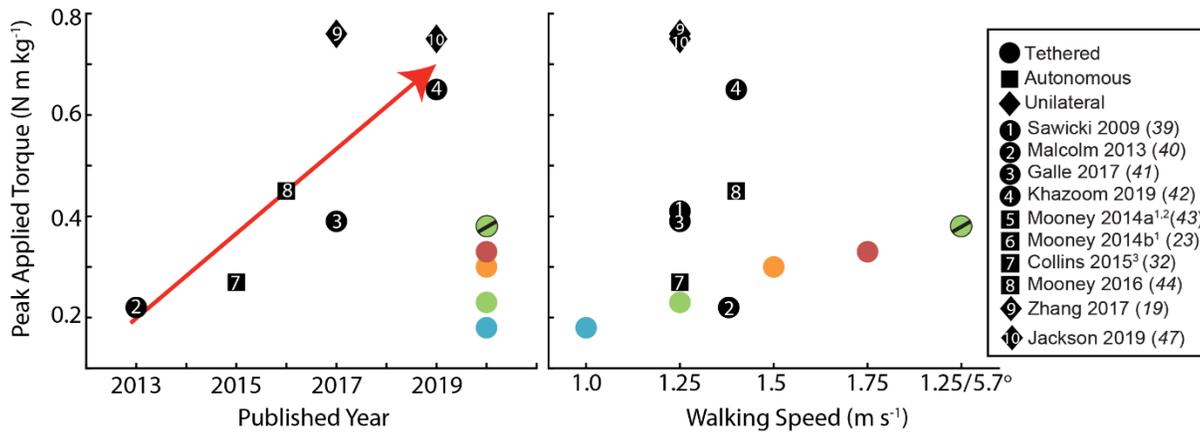
Fig. S7. Peak force applied in prior studies compared to the MBA profile. (Left) Peak applied torque in reference studies from the past 10 years. **(Right)** Same studies denoting the walking speed and incline. For context, to generate 0.8 N m kg^{-1} requires approximately 560 N of force (70 kg, 0.1m moment arm) which must be reacted against the skin in soft exosuits. Profile references 9 and 10 are unilateral/tethered and metabolic demand are compared to slack (thus referenced here but not in metabolic comparison). (Notes: [1]Exoskeleton torque not reported; [2]Walking with load carriage; [3]Passive device)

1020   **Table S1. Muscle-Tendon Mechanics**

	Walking Condition				
	1 m s⁻¹	**1.25 m s⁻¹**	**1.5 m s⁻¹**	**1.75 m s⁻¹**	**5.7º**
Peak Sol Vel (mm/s)	20.81 ± 4.4	29.23 ± 4.69	37.44 ± 4.98	39.38 ± 4.62	39.15 ± 3.84
Sol Stretch @ 60% (mm)	2.38 ± 0.53	3.98 ± 0.67	6.26 ± 0.88	8.65 ± 1.16	7.89 ± 0.97
Force @ 60% (N)	89.65 ± 16.76	148.03 ± 20.34	238.75 ± 26.69	328.47 ± 28.99	295.84 ± 18.38
MBA Onset (% stride)	45.5 ± 2.9	41.8 ± 2.5	34.5 ± 2.9	32.5 ± 2.2	31.1 ± 1.9
MT (Joint) Positive Power Onset (% stride)	52.9 ± 1.57	51.2 ± 1.71	49.5 ± 1.71	49.1 ± 0.78	49.7 ± 1.93

Data are mean ± s.e.m.

Table S2. Ankle and Exo Dynamics

			Walking Condition				
			1 m s⁻¹	**1.25 m s⁻¹**	**1.5 m s⁻¹**	**1.75 m s⁻¹**	**5.7°**
Ankle Moment	Mean Stride	ND	0.35 ± 0.02	0.36 ± 0.02	0.36 ± 0.02	0.36 ± 0.02	0.41 ± 0.02
		MBA	0.36 ± 0.01	0.37 ± 0.01	0.37 ± 0.01	0.38 ± 0.02	0.39 ± 0.02
	Peak	ND	1.52 ± 0.03	1.68 ± 0.03	1.83 ± 0.04	1.97 ± 0.05	1.9 ± 0.03
		MBA	1.52 ± 0.03	1.66 ± 0.04	1.79 ± 0.05	1.99 ± 0.06	1.88 ± 0.03
Ankle Power	Mean Stride	ND	-0.02 ± 0.01	0.03 ± 0.02	0.1 ± 0.02	0.18 ± 0.02	0.18 ± 0.02
		MBA	**0.08 ± 0.02**	**0.19 ± 0.02**	**0.31 ± 0.02**	**0.43 ± 0.03**	**0.34 ± 0.01**
	Peak	ND	2.32 ± 0.12	3.27 ± 0.19	4.13 ± 0.19	5.05 ± 0.26	3.91 ± 0.2
		MBA	**3.14 ± 0.19**	**4.9 ± 0.32**	**6.73 ± 0.56**	**8.41 ± 0.45**	**6.09 ± 0.35**
Exo Moment	Mean Stride	ND	0 ± 0	0 ± 0	0 ± 0	0 ± 0	0 ± 0
		MBA	**0.03 ± 0**	**0.03 ± 0**	**0.03 ± 0**	**0.04 ± 0**	**0.05 ± 0**
	Peak	ND	0 ± 0	0 ± 0	0 ± 0	0 ± 0	0 ± 0
		MBA	**0.18 ± 0.03**	**0.23 ± 0.03**	**0.3 ± 0.03**	**0.33 ± 0.03**	**0.38 ± 0.03**
Exo Power	Mean Stride	ND	0 ± 0	0 ± 0	0 ± 0	0 ± 0	0 ± 0
		MBA	**0.05 ± 0.01**	**0.06 ± 0.01**	**0.08 ± 0.01**	**0.09 ± 0.01**	**0.07 ± 0.01**
	Peak	ND	0 ± 0	0 ± 0	0 ± 0	0 ± 0	0 ± 0
		MBA	**1 ± 0.23**	**1.49 ± 0.24**	**1.93 ± 0.28**	**2.25 ± 0.23**	**1.73 ± 0.21**
Bio Moment	Mean Stride	ND	0.35 ± 0.02	0.36 ± 0.02	0.36 ± 0.02	0.36 ± 0.02	0.41 ± 0.02
		MBA	0.33 ± 0.01	0.34 ± 0.01	**0.33 ± 0.01**	0.34 ± 0.02	**0.34 ± 0.02**
	Peak	ND	1.52 ± 0.03	1.68 ± 0.03	1.83 ± 0.04	1.97 ± 0.05	1.9 ± 0.03
		MBA	1.48 ± 0.03	**1.58 ± 0.04**	**1.63 ± 0.06**	**1.77 ± 0.07**	**1.61 ± 0.05**
Bio Power	Mean Stride	ND	-0.02 ± 0.01	0.03 ± 0.02	0.1 ± 0.02	0.18 ± 0.02	0.18 ± 0.02
		MBA	**0.04 ± 0.01**	**0.12 ± 0.01**	**0.23 ± 0.02**	**0.35 ± 0.02**	**0.26 ± 0.01**
	Peak	ND	2.32 ± 0.12	3.27 ± 0.19	4.13 ± 0.19	5.05 ± 0.26	3.91 ± 0.2
		MBA	**2.72 ± 0.14**	**4.06 ± 0.23**	**5.35 ± 0.45**	**6.78 ± 0.59**	**4.57 ± 0.28**
Ankle Angle	Peak DF	ND	20.8 ± 1.04	20.15 ± 0.84	19.08 ± 0.92	17.11 ± 0.68	22.91 ± 0.97
		MBA	20.51 ± 1.22	19.58 ± 1.35	18.83 ± 1.22	16.44 ± 1.7	22.29 ± 0.95
	Peak PF	ND	-5.26 ± 1.32	-7.51 ± 1.28	-10.1 ± 1.1	-11.6 ± 1.51	-6.59 ± 1.09
		MBA	**-14.36 ± 1.97**	**-15.09 ± 2.03**	**-15.49 ± 1.2**	**-17.17 ± 1.73**	**-9.71 ± 1.06**
Ankle Velocity	Peak DF	ND	107.11 ± 9.81	135.52 ± 11.46	172.33 ± 10.35	158.62 ± 9.7	129.03 ± 9.98
		MBA	**173.03 ± 31.5**	169.46 ± 33.68	181.77 ± 13.03	162.83 ± 4.37	**144.51 ± 12.1**
	Peak PF	ND	-203.28 ± 11.76	-244.52 ± 12.58	-293.06 ± 11.68	-273.1 ± 13.69	-229.14 ± 8.52
		MBA	**-320.93 ± 26.86**	**-377.35 ± 27.44**	**-433.62 ± 26.39**	**-386.14 ± 20.18**	**-282.55 ± 21.59**

Data are mean ± s.e.m. Bold signifies a significant change of MBA compared to NO-DEVICE (ND) at that walking task (paired t-test p < 0.05). Underline further indicates the use of Wilcoxon Signed Rank due to non-normally distributed data.

1030 **Table S3. Individual Metabolic Response**

					Walking Condition					
	1 m s⁻¹		**1.25 m s⁻¹**		**1.5 m s⁻¹**		**1.75 m s⁻¹**		**5.7°**	
Participant	No-Dev	MBA	No-Dev	MBA	No-Dev	MBA	No-Dev	MBA	No-Dev	MBA
1	4.24	2.49	4.97	3.19	6.72	4.71	9.18	7.31	11.25	8.14
2	3.21	3.22	4.28	4.12	5.60	5.66	8.54	7.85	9.49	8.38
3	4.23	3.98	5.67	3.68	6.28	5.44			9.07	8.28
4	2.16	2.41	2.81	2.72	3.79	3.51	4.90	4.34	6.63	6.12
5	2.22	1.78	3.00	2.40	4.50	4.32	7.05	6.05	7.85	8.01
6	2.45	2.10	3.62	2.87	5.11	4.23			7.92	7.35
7	2.65	2.82	3.93	3.11	4.34	4.60	6.99	6.78	8.57	8.76
8	1.59	1.95	3.01	2.89	4.23	3.91	6.24	5.53	8.17	7.48
9	2.54	2.60	3.41	3.42	4.63	3.99	5.68	6.05	7.69	7.44
Mean	2.81	2.59	3.86	3.15	5.02	4.48	6.94	6.27	8.52	7.77
Std Error	0.31	0.23	0.32	0.17	0.33	0.24	0.51	0.39	0.44	0.26
n	9		9		9		7		9	
Z	-5		-22		-18.5		-12		-19.5	
	p = 0.5859		p = 0.0078		p = 0.0273		p = 0.0468		p = 0.0195	

We used the Wilcoxon Signed Rank test due to non-normally distributed data.

Table S4. Muscle Activation

			Walking Condition				
			1 m s^{-1}	**1.25 m s^{-1}**	**1.5 m s^{-1}**	**1.75 m s^{-1}**	**5.7°**
Soleus	Mean Stride	ND	0.14 ± 0.01	0.17 ± 0.01	0.2 ± 0.01	0.23 ± 0.01	0.22 ± 0.02
		MBA	0.13 ± 0.01	0.17 ± 0.01	0.2 ± 0.01	0.22 ± 0.02	0.2 ± 0.01
	Mid/Late Stance	ND	0.3 ± 0.03	0.39 ± 0.03	0.46 ± 0.03	0.52 ± 0.01	0.48 ± 0.03
		MBA	**0.28 ± 0.02**	**0.36 ± 0.02**	**0.42 ± 0.03**	**0.48 ± 0.03**	**0.43 ± 0.03**
	Peak	ND	0.51 ± 0.03	0.66 ± 0.04	0.8 ± 0.04	0.91 ± 0.03	0.92 ± 0.04
		MBA	0.46 ± 0.02	0.59 ± 0.03	0.74 ± 0.04	0.84 ± 0.04	0.84 ± 0.04
Tibialis Anterior	Mean Stride	ND	0.13 ± 0.02	0.16 ± 0.02	0.19 ± 0.02	0.22 ± 0.02	0.16 ± 0.02
		MBA	0.12 ± 0.01	**$\underline{0.14 \pm 0.01}$**	0.19 ± 0.01	0.22 ± 0.01	0.17 ± 0.02
	Peak	ND	0.51 ± 0.04	0.64 ± 0.04	0.81 ± 0.05	0.95 ± 0.05	0.57 ± 0.04
		MBA	0.48 ± 0.04	0.61 ± 0.05	0.81 ± 0.05	0.95 ± 0.02	0.6 ± 0.04

Data are mean ± s.e.m. Bold signifies a significant change of MBA compared to NO-DEVICE (ND) at that walking task (paired t-test $p < 0.05$). Underline further indicates the use of Wilcoxon Signed Rank due to non-normally distributed data.

Table S5. Spatiotemporal Data

			Walking Condition				
			1 m s^{-1}	**1.25 m s^{-1}**	**1.5 m s^{-1}**	**1.75 m s^{-1}**	**5.7°**
Spatio-temporal	Stride Time	ND	1.19 ± 0.01	1.07 ± 0.01	0.99 ± 0.01	0.93 ± 0.01	1.11 ± 0.02
		MBA	1.21 ± 0.02	1.1 ± 0.01	**1.02 ± 0.01**	0.94 ± 0.01	1.14 ± 0.02
	Stance Time	ND	0.78 ± 0.01	0.69 ± 0.01	0.62 ± 0.01	0.58 ± 0.01	0.72 ± 0.01
		MBA	0.8 ± 0.02	0.7 ± 0.01	**0.64 ± 0.01**	0.58 ± 0.01	0.72 ± 0.01
	Duty	ND	65.96 ± 0.46	63.92 ± 0.31	62.74 ± 0.22	61.77 ± 0.45	64.87 ± 0.31
		MBA	65.97 ± 0.41	64.31 ± 0.48	62.89 ± 0.5	61.33 ± 0.43	**63.27 ± 0.46**

Data are mean ± s.e.m. Bold signifies a significant change of MBA compared to NO-DEVICE (ND) at that walking task (paired t-test $p<0.05$).

1040